Studying the Diffusion of Al^{3+} ions from Atomic Layer Deposited Al_2O_3 Surface Coatings into Positive Electrode Materials and the Effects Thereof Using Full Coin Cells

by

Vivian Murray

Submitted in partial fulfilment of the requirements
for the degree of Master of Applied Science

at

Dalhousie University
Halifax, Nova Scotia
February 2019

TABLE OF CONTENTS

LIST OF FIGURES

ABSTRACT

Increasing the energy density of lithium-ion batteries (LIBs) is an important goal for battery research for electric vehicle and grid storage applications. One method of doing this is to use a protective coating on the positive electrode material to protect against electrode/electrolyte reactions that occur as the charging voltage of the cells is increased, which increases energy density. This work develops methods to prepare full coin cells and uses these methods to examine the effectiveness of Al_2O_3 coatings prepared by atomic layer deposition (ALD). Two coating thicknesses on two positive electrode materials, $LiNi_{0.6}Mn_{0.2}Co_{0.2}O_2$ (NMC622) and $LiNi_{0.8}Co_{0.15}Al_{0.05}O_2$ (NCA801505), were examined. Samples annealed to various temperatures were characterized using scanning electron microscopy (SEM), ^{27}Al magic angle spinning solid-state nuclear magnetic resonance spectroscopy (ssNMR), and X-ray photoelectron spectroscopy (XPS). ssNMR on the thick-coated NMC series suggests Al^{3+} diffusion into the NMC material occurs at annealing temperature $\geq 400^{\circ}C$. However, XPS results only show signs of Al^{3+} diffusion at $\geq 600^{\circ}C$ for the thin-coated material and $\geq 700^{\circ}C$ for the thick-coated material. This apparent disagreement occurs because the Al_2O_3 coatings are thicker than the XPS measurement depth and so the initial diffusion from the coating is not visible to XPS. As the annealing temperature increases, so does the diffusion rate of the Al_2O_3 layer into the NMC. Thus, the coating layer thickness is reduced below the XPS measurement depth at higher temperatures. Full coin cells prepared from the ALD-coated materials show that for both NMC and NCA materials with the thicker Al_2O_3 coating, annealing to 600°C provides the best cycling results.

LIST OF ABBREVIATIONS USED

ALD	Atomic layer deposition
BMF	Polypropylene blown micro fiber
DEC	Diethyl carbonate
EC	Ethylene carbonate
LIB	Lithium ion batteries
$LiMO_2$	Lithium transition metal oxide
MAS	Magic angle spinning
NCA0801505	$Li[Ni_{0.8}Co_{0.15}Al_{0.05}]O_2$
NMC622	$Li[Ni_{0.6}Mn_{0.2}Co_{0.2}]O_2$
NMP	N-methyl 2-pyrrolidone
NMR	Nuclear magnetic resonance spectroscopy
p	Fraction of graphene layers in turbostratic misalignment
PVDF	Polyvinylidene difluoride
SEI	Solid electrolyte interphase
SEM	Scanning electron microscopy
ssNMR	Solid state nuclear magnetic resonance spectroscopy
TMA	Trimethylaluminum
XPS	X-ray photoelectron spectroscopy

ACKNOWLEDGEMENTS

I would like to thank Tesla Canada and NSERC for the funding of my work.

I would like to thank my supervisor, Dr. Jeff Dahn, for all of his support, guidance, knowledge, help, and patience. I am very lucky to have had the opportunity to learn from him and experience first-hand his passion for research.

I would like to thank all of the Dahn lab members, without which I would have been lost. Thank you for all of the help and encouragement.

Thank you to my friends and family for all of the love and support that made this possible and to the friends I made in Halifax who made my time there so incredible.

And last, but definitely not least, thank you to Rich for all of the endless love and encouragement.

CHAPTER 1 INTRODUCTION

1.1 JUSTIFICATION

Lithium ion Batteries (LIBs) are widely used in a variety of consumer products. With their rising use in electric vehicles and grid storage applications, increasing the energy density of LIBs is a key goal for energy storage researchers. One approach is to develop new positive electrode materials that have higher specific capacities and that are stable at higher operational cell voltages[1,2,3,4,5,6]. This thesis will look at one method of making positive electrode materials more stable at higher voltages by using a protective coating layer. This would allow for more energy to be stored in a battery without increasing its size. Additionally, this thesis will present an optimized method for reliable testing of new positive electrode materials using full coin cells.

1.2 SCOPE OF THESIS

Chapter 2 presents an introduction to lithium ion cells. The basic components are discussed as well as the various types of cells used in this thesis. Finally, lithium ion cell degradation is discussed to further explain the function of protective coatings on positive electrode materials. Chapter 3 discusses the experimental procedures used in this thesis. This includes electrolyte preparation, pouch cell preparation, electrode materials preparation, electrode fabrication, coin cell fabrication, electrochemical testing procedures and other characterization methods. Chapter 4 presents the process of optimizing the fabrication of full coin cells and Chapter 5 discusses the results of the study of the coated materials. The materials were studied using scanning electron microscopy (SEM), x-ray photoelectron spectroscopy (XPS), solid state nuclear magnetic resonance spectroscopy

(ssNMR), and finally evaluated using the full coin cell process from Chapter 4. Chapter 6 presents the conclusions and makes suggestions for future work.

The work presented in Chapter 4 was previously published in a peer-reviewed journal article: V. Murray, D. S. Hall, and J. R. Dahn, J. Electrochem. Soc., 166, A329–A333 (2019). doi: 10.1149/2.1171902jes. The article was published as an open access article and therefore no license agreement is required to reproduce this previously published work.

The work presented in Chapter 5 was submitted to Tesla for approval to publish in December 2018. Approval has not yet occurred but is expected soon.

CHAPTER 2 LITHIUM ION BATTERIES

2.1 LITHIUM ION CELLS

Batteries are a combination of two or more electrochemical cells that convert chemical potential into electrical potential through redox reactions. There are two classes of batteries, primary batteries which are not rechargeable, and secondary batteries, which are. Lithium ion batteries (LIB) belong to the secondary class and are comprised of many lithium ion cells connected in series and parallel. During discharge of a cell, lithium ions move spontaneously from the negative electrode to the positive electrode through the electrolyte while the corresponding electrons move through the external circuit, producing electrical energy. During charge of a cell electrical energy is applied to move the lithium ions and electrons in the opposite direction.

A lithium-ion cell is composed of four main components. A positive electrode, a negative electrode, an electrolyte, and a separator, as shown in Figure 2.1. The electrolyte allows the lithium ions to move between electrodes, while the electrodes are layered materials that allow for the reversible insertion or removal of lithium ions between layers. This is called intercalation or deintercalation, respectively.

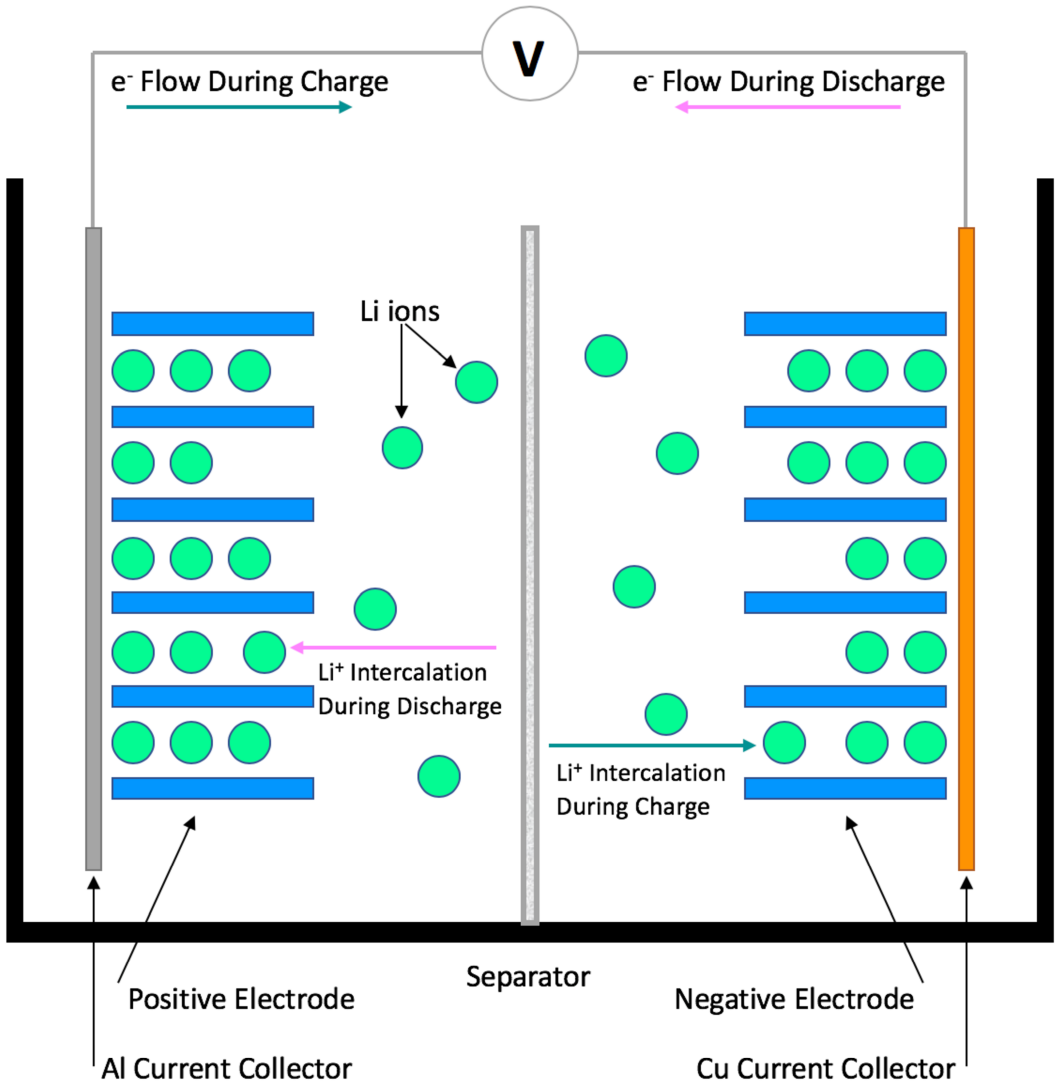

Figure 2.1: Schematic of a lithium ion cell during charge and discharge

During discharge of the battery, spontaneous redox reactions result in lithium ions deintercalating from the negative electrode, traveling through the electrolyte and intercalating into the positive electrode. The separator in the battery allows the lithium ions to pass through but blocks the passage of electrons. This forces the electrons to travel through the external circuit, creating a current as shown in Figure 2.1. During charging of the battery, the lithium ions move in the opposite direction. They deintercalate from the

positive electrode and intercalate into the negative electrode. This is not spontaneous and requires electrical energy to be applied to the cell during charging. The following equations outline the redox reactions that occur during charge and discharge at the positive and negative electrodes. The equations proceed in the forward direction during discharge and the reverse during charge. In Equation 1, during discharge, lithium is oxidized and deintercalates from graphite (C_6). In Equation 2, during discharge, lithium is reduced and intercalates into the lithium transition metal oxide ($LiMO_2$)[7].

$$yLi_{x/y}C_6 \leftrightarrow yC_6 + xLi^+ + xe^- \quad [1]$$

$$Li_{1-x}MO_2 + xLi^+ + xe^- \leftrightarrow LiMO_2 \quad [2]$$

Three important terms used in describing LIBs are voltage, capacity, and C-rate. As lithium ions move through the cell, the potentials of the positive and negative electrodes, with respect to a fixed potential like Li/Li^+, change. Voltage is a potential difference so the voltage of a full cell is the difference in potential of the positive and negative electrodes and changes during charge and discharge. A cell is at its highest voltage when fully charged. The capacity of a cell, measured in Ah or mAh, is relative to the number of electrons that move throughout the cell. Because this is equal to the number of lithium ions that move between electrodes, anything that decreases the amount of available lithium in the cell decreases the available capacity of the cell. Specific capacity is similar except it is measured in mAh per gram of active material in an electrode. This allows for direct comparison of performance of electrode materials on a gravimetric basis. C-rate refers to the current at which a cell is cycled. It is the capacity of the cell in mAh divided by the

number of hours it would take for the cell to be charged or discharged. Two C-rates are typically used when cycling cells, a lower C-rate for the formation cycle (here C/5 or C/10) and then a slightly higher rate is used for cycling (here C/3 or C/5). As an example, if a C/3 current is selected it will take 3 hours for a cell to discharge and 3 hours for a cell to charge.

2.2 LITHIUM ION CELL COMPONENTS

2.2.1 Positive Electrode Materials

Positive electrodes typically contain three ingredients. A binder, such as polyvinylidene difluoride (PVDF), which helps the electrode material adhere to the aluminum current collector, a conductive agent, such as carbon black, which enhances the conductivity of electrode, and the active material. The active material comprises approximately 92 – 96% of the electrode although the exact composition may vary[8]. The active material is typically a lithium transition metal oxide, $LiMO_2$. The most common structure is a layered structure that allows for intercalation of lithium ions in between layers. Spinel and olivine structures are other alternatives[7,9].

The first LIBs produced used $LiCoO_2$, however due to rising costs and supply issues with cobalt, a mixture of transition metals has become a popular alternative to using only cobalt as the transition metal[10,11]. Of the current commonly used materials, the two that are used in this thesis are $LiNi_{0.6}Mn_{0.2}Co_{0.2}O_2$ (NMC622) and $LiNi_{0.8}Co_{0.15}Al_{0.5}O_2$ (NCA801505).

2.2.2 Negative Electrode Materials

Negative electrodes are typically made of graphite. Graphite is a layered structure consisting of layers of graphene sheets in parallel alignment. The lithium ions reversibly intercalate between the sheets. There are two types of graphite, natural graphite and artificial or synthetic graphite, used in this thesis. An important factor in performance of graphite is the degree of turbostratic misalignment, p between adjacent graphene layers. This refers to the degree that the layers are arranged with p=1 indicating that every sheet is misaligned and p=0 indicating that the probability of finding two adjacent sheets misaligned drops to 0. Natural graphite has a low degree of turbostratic misalignment whereas artificial graphite needs to be pyrolyzed (heated to high temperature under inert gas) to reduce the degree of misalignment and improve performance[12,7,13,14].

2.2.3 Electrolyte

Electrolytes have two main components, a salt, which is usually $LiPF_6$, dissolved in what is typically a mixture of organic solvents. A large amount of research into advancing LIB technology is focused on the electrolyte, and small changes can have large impacts on performance. Often additives are used that are only a few percent by weight of the electrolyte solution but can greatly impact cell performance and lifetime. A well performing electrolyte should be conductive and therefore have a high dielectric constant, have low viscosity, be useful in a wide range of temperatures, and have good stability at the operating voltages of both electrodes[7,15].

2.2.4 Separator

The separator acts to prevent contact between the positive and negative electrodes, which would result in a short circuit. Ions can pass through the separator however electrons cannot and are therefore forced to follow the external circuit. The separator also acts as a safety mechanism. In the case of thermal runaway, the separator will melt preventing ion transfer. Separators are typically made of polyethylene, polypropylene, or a combination[7]. Two types are used in this thesis, Celgard 2320 thin film polypropylene microporous films (Celgard) and Polypropylene Blown Micro Fiber (BMF) separator (3M).

2.2.5 Cell Types

There are several types of LIB construction used in industry and research. The two types used in this thesis are pouch cells and coin cells. A pouch cell has the same general construction as another popular type, the cylindrical cell. In both cases the positive electrode, negative electrode, and separator are wound together in a "jelly roll". The main difference is the casing which is either a pouch bag or metal can, respectively. In both cases the positive and negative electrodes are double sided to maximize the amount of active material in the cell. When studying new electrolyte formulations or additives, pouch cells are usually used in our laboratory. They are machine manufactured in large batches and just need to be filled with the electrolyte in question to be used in electrochemical testing. Further details on this process are given in Chapter 3.2. Pouch cells, however, are not practical to use when studying new electrode materials. As they are machine manufactured in large batches there is a large upfront cost to making ones with a new electrode material. Coin cells are more often used in investigating new electrode materials. There are two

variations of coin cells, half coin cells and full coin cells, both of which are discussed further in Chapter 3. In both cases, the positive electrode is made in a laboratory and the coin cell is manually constructed in a glove box. As these are handmade instead of machine manufactured there is inherently more variation between cells however they are the best option when studying new electrode materials. Chapter 4 of this thesis will present an optimized method of producing reliable full coin cells.

2.3 LITHIUM ION CELL DEGRADATION

As LIBs age their components degrade. Primarily this is a result of reactions between the electrolyte and either the positive or negative electrode. Two such instances are discussed in this section[7].

2.3.1 Solid Electrolyte Interphase (SEI)

The SEI is essential to the performance of a LIB. It is formed by the products of a parasitic reaction between the electrolyte and electrode that create a passivating layer on the electrode surface. This layer allows lithium ions to move through but hinders and hopefully prevents further reactions between the electrode and electrolyte[7,16]. The SEI layer forms primarily on the first cycle, which is why it is often referred to as the formation cycle. The SEI layer does continue to grow as the cell is cycled, however its growth is approximately proportional to $(time)^{1/2}$, so the rate slows with time as does the amount of lithium ions consumed by formation of the layer[17]. Continual growth of the layer will continue to reduce the amount of available lithium ions and will contribute to further degradation of the cell[18].

2.3.2 Preventative Protective Coatings

The primary focus of this thesis, found in Chapter 5, presents a study of the use of a protective coating on the positive electrode to prevent several degradation processes that can occur at high potential including transition metal dissolution[19,20,21] oxygen loss[22,23,24] and reactions between the positive electrode and the electrolyte[25,26]. These processes can consume lithium ions or electrolyte and therefore reduce the available capacity of the cell. Furthermore, they also create increased cell impedance due to the ever-thickening SEI layers. If these reactions can be prevented or at least slowed down then the lifetime of the cell can be extended while also allowing it to be operated at higher voltages.

The benefits of several inorganic coatings have been previously investigated including MgO[27], TiO_2[28,29], SiO_2[30,31], Li_2ZrO_3[32], and Al_2O_3[33,34,35,36,37,38,39,40,41,42,43,44]. The most common method of depositing the coating on positive electrode materials is through a wet chemistry method which can vary in details and precursors used so a general guideline to the procedure is outlined here. Typically the powered positive electrode materials are added to a solution that includes the Al precursor, usually a soluble aluminum salt or alkoxide, dissolved in a solvent. The ratio between Al precursors and positive electrode material is selected to produce a final weight percent ratio of the coating. The solution is stirred at room temperature for 0-6 hours and then stirred at 80°C for an additional 12-48 hours to evaporate the solvent from the solution. The remaining mixture is then dried under vacuum for 4 hours[38,39,45]. These methods are generally easy to scale up and cost efficient, however they can produce thick, uneven coatings[35,37,38]. Another

drawback of the wet chemistry methods is that they can result in an initial decrease in capacity by drawing Li from the bulk material[39].

An alternative method of depositing the coating is to use atomic layer deposition (ALD). Riley et al[43] studied the effect of coating thickness of ALD Al_2O_3 on $LiNi_{1/3}Mn_{1/3}Co_{1/3}O_2$, comparing uncoated material to that with 2, 4, 6, 8 or 10 layers of ALD Al_2O_3 coating. They found the only thickness to perform worse than the uncoated material was that with 10 layers of ALD and that the best performing coating thickness was 2 layers of ALD (or approximately 4 Å). This suggests that thinner surface coatings generally result in better performing cells. It has also been shown that the ALD method of depositing coatings produces an extremely precise, even and ultrathin layer[42]. Although ALD has traditionally been prohibitively expensive[41,42,43,46,47], recently the costs associated with ALD have decreased, possibly making it a viable alternative to the traditional wet chemistry methods.

During the ALD process, the coating is applied in layers and with each layer applied there are several steps. A gaseous precursor is pumped into a chamber under vacuum. The gaseous precursor then reacts with the substrate surface, creating a monolayer on the surface. To remove any unwanted biproducts or unreacted precursor the chamber is then purged with an inert gas. These two steps are then repeated with a gaseous counter-reactant precursor. This results in one layer of coating and can be repeated as necessary[48].

When depositing Al_2O_3 ALD films, the precursors are trimethylaluminum (TMA) and H_2O. The overall reaction for the deposition of Al_2O_3 is:

$$2Al(CH_3)_3 + 3H_2O \rightarrow Al_2O_3 + 6CH_4 \quad [3]$$

For each layer of growth each precursor (TMA and H_2O) is exposed to the substrate in two separate half reactions. The reactions responsible for growth are listed below in equations 4 and 5.

$$AlOH^* + Al(CH_3)_3 \rightarrow AlO–Al(CH_3)^*_2 + CH_4 \quad [4]$$

$$AlO–Al(CH_3)^*_2 + H2O \rightarrow AlO–Al–OH^* + CH_4 \quad [5]$$

Here the asterisks indicate a surface species[49,50,51,52,53,42]. Each layer is applied by alternating the two reactions and therefore the amount of layers, or thickness of coating, can be controlled. A diagram of this can be found below in Figure 2.2.

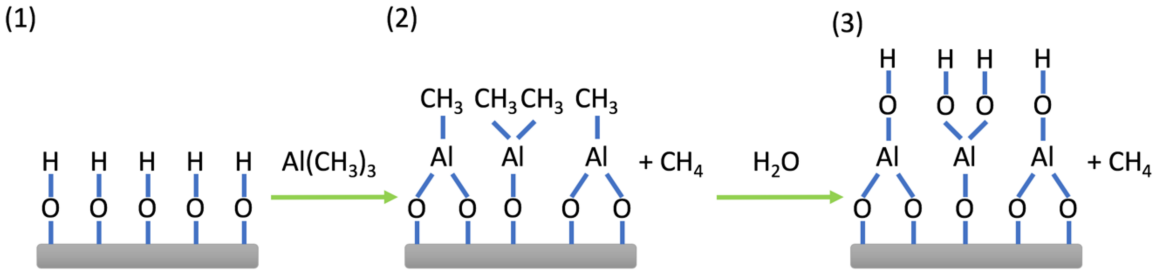

Figure 2.2: Schematic of one layer of Al_2O_3 ALD according the reactions given above. Before step 2, and in between every subsequent step, the chamber is flushed with an inert gas to remove reaction byproducts and unreacted precursor (not shown)[50].

Previous research on coatings deposited using wet chemistry methods have found that after coating the positive electrode material, annealing the sample improves performance of the resulting cells[39,45]. While in principle it is possible that the Al_2O_3 in the

coating could react with Li in the positive electrode materials as shown in the phase diagram in Figure 2.3[54], it is suggested in this work that the Al^{3+} from the coating diffuses into the positive electrode material.

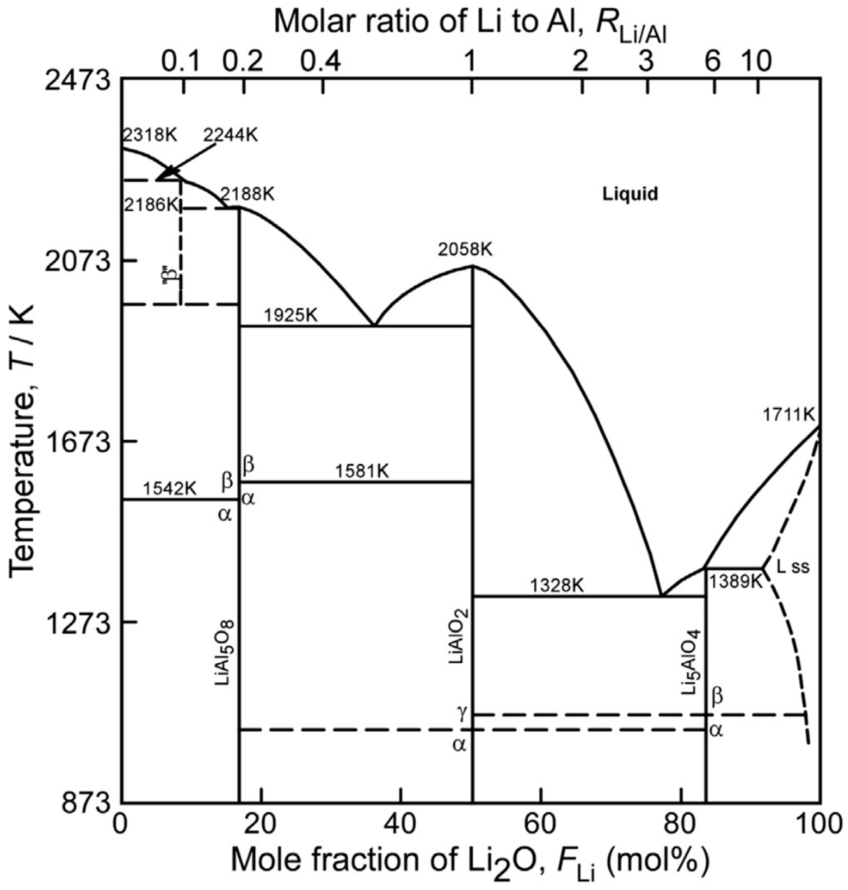

Figure 2.3: Phase diagram of Li-Al-O system. Figure from a 2013 by Chi et al.[54], reproduced with permission from *The Journal of Materials Chemistry and Physics*, **143**, 1338–1343 (2014). Copyright 2013, Elsevier B.V.

In Chapter 5 the results of characterization and electrochemical testing on ALD Al_2O_3 coatings on both $LiNi_{0.6}Mn_{0.2}Co_{0.2}O_2$ (NMC622) and $LiNi_{0.8}Co_{0.15}Al_{0.5}O_2$ (NCA801505) will be presented. The effects of annealing temperature and coating thickness will be discussed.

CHAPTER 3 EXPERIMENTAL METHODS

3.1 POUCH CELL PREPARATION

Machine-made pouch cells used in this thesis were 240 mAh NMC622/graphite 402035-size cells obtained dry (no electrolyte) from Li-Fun Technology Co. (Zhuzhou City, China). The pouch cells were vacuum sealed, without electrolyte, in a dry room in China and then shipped to Canada for our use. The NMC622 material was coated with Al_2O_3, (not using ALD, but the exact method is unknown to us) and is called "NMC622A" in the paper by Jing Li et al, where extensive tests in full Li-ion pouch cells are reported[55]. The positive electrodes had a mass loading of 21.3 mg/cm^2 and the coating was pressed to a density of 3.3 g/cm^2. The electrode formulation was 96% active material, 2% PVDF binder and 2% Super S carbon black conducting diluent by weight. Such an electrode formulation is similar to those promoted by Marks et al[8]. The graphite (AML-400 grade from Kaijin, China) negative electrodes had a loading of 13.2 mg/cm^2 and the coating was pressed to a density of 1.55 g/cm^2. The electrode formulation was 96% active material, 2% CMC/SBR binder and 2% Super S carbon black conducting diluent by weight.

The pouch cells were filled with 1.0 ± 0.02 g of electrolyte solution, sealed at -90 kPa gauge pressure using a compact vacuum sealer (MSK-115A, MTI Corp.) and immediately held at 1.5 V at room temperature (21 – 25°C) to prevent corrosion of the copper current collector during the ~24 h wetting period that followed. Cells were then loaded into temperature-controlled boxes (30.0 ± 0.1°C) and connected to a Maccor 4000 Series automated test system (Maccor Inc.). Because gas formation was expected to occur during formation, the pouch cells were clamped using soft rubber (at about 25 kPa gauge pressure), which has previously been observed to significantly improve the experimental

precision[56]. Following the first full cycle (i.e., the formation cycle) between 2.8 – 4.3 V and at ~C/10, cells were charged to 3.8 V and stopped. Cells were cut open in an argon-atmosphere glove box and vacuum sealed again in order to remove the gas produced during formation. Finally, cells were taken for cycling testing.

3.2 ELECTRODE MATERIALS PREPARATION

Multiple samples of positive electrode materials were received from the Forge Nano Company (1172 W Century Dr, Louisville, CO 80027). These included several variations of two positive electrode materials, NMC622 and NCA801505. For each positive electrode material, an uncoated, pristine, sample was received to be used as a reference. Additionally, for both NMC622 and NCA801505, two separate coating thicknesses were received. The coatings were Al_2O_3 deposited using ALD through a proprietary method resulting in two different thicknesses. As a result the exact thicknesses are unknown, however it is known that they are on the order of nanometers and that one is relatively thicker than the other. Therefore, there are six different sample categories, a pristine, a thick-coated, and a thin-coated sample for each of the two positive electrode materials, NMC622 and NCA801505. Samples from each of the four coated materials were then heat treated, in air, to temperatures ranging from 400°C to 900°C for one hour. Once the samples had cooled to 400°C they were moved into glass jars, “sealed” with parafilm wax and used immediately after opening to minimize contact with air and moisture.

3.3 ELECTRODE FABRICATION

Two different methods of preparing electrodes for full coin cells were used in this thesis. The first method described was used to evaluate the construction of full coin cells and used materials from machine made pouch cells. The second method described was used to evaluate the electrochemical performance of the ALD coated positive electrode materials and used positive electrodes made from these materials combined with machine made negative electrodes. All electrodes were punched with a diameter of 1.27 cm.

In order to evaluate and optimize the construction method of full coin cells, machine made electrodes were used to eliminate the possibility of variance in hand made electrodes. Positive and negative electrodes were punched from the single sided region of unwound pouch cells described above. The electrodes were punched in air and then heated under vacuum in a glovebox antechamber overnight at 110°C before being transferred into the glove box.

To evaluate the electrochemical performance of the ALD coated positive electrode materials, electrodes were prepared from these materials and then used to form full coin cells. The positive electrodes made from Forge Nano materials were made using the formulation promoted by Marks et al.[8] Positive electrodes were made by depositing a slurry containing 92% active material, 4% Super-S carbon black, 4% Polyvinylidene difluoride binder (PVDF), and mixed with N-methyl 2-pyrrolidone (NMP) spread on an Al foil current collector with a 279 μm notch bar. The electrodes were then dried in an oven at 110°C for 12 hours before being calendared at a pressure of 2000 atm. Electrodes were punched and then heated under vacuum at 110°C for 14 hours before being transferred into the glove box. The positive electrodes have an average loading of 15 mg/cm^2.

Negative electrodes were punched from a single-sided graphite electrode deposited on a Cu foil current collector supplied by Tesla. They were then heated under vacuum at 110°C for 14 hours.

3.4 COIN CELL FABRICATION

Full cells were constructed with one of the two configurations shown in Figure 3.1. In Figure 3.1a, two Celgard separators were used and in Figure 3.1b, one BMF (Polypropylene Blown Micro Fiber available from 3M Company) separator was used. The BMF separators are about 0.25 mm thick, about 90% porous and are very soft and compliant. For each material at least two repeats of each cell were made.

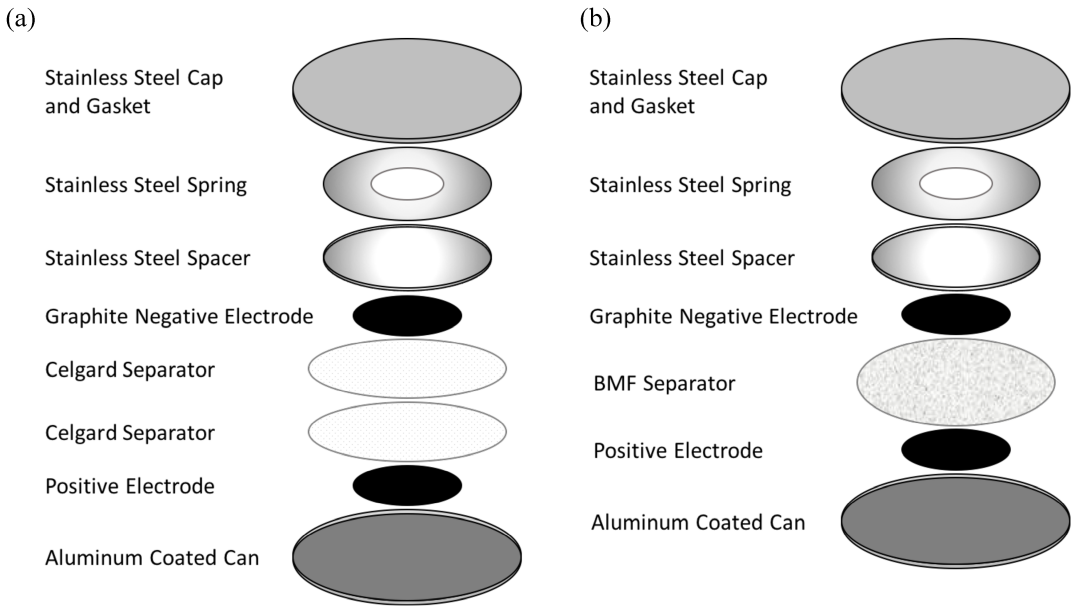

Figure 3.1: Diagram of Full Cell with (a) Two Celgard separators or (b) One BMF Separator.

Some of the cells were constructed with the help of a vacuum pen (Virtual Industries, V8901), as discussed in the main text of this article. Figure 3.2 shows the exact model used.

Figure 3.2: Vacuum Pen (Virtual Industries, V8901[57])

After cycling some of the cells were disassembled to check for electrode alignment issues to help explain observed testing behavior.

3.5 SCANNING ELECTRON MICROSCOPY

The morphology of the cathode materials used in this work was imaged using a Hitachi S-4700 scanning electron microscope. Residual lithium carbonate was removed by washing samples three times in a 4:1 ratio, by volume, with high purity water (≥ 18.2 MΩ cm, Barnstead NANOpure) and centrifuging to collect the powder. After rinsing and drying, powder samples were mounted on double-sided adhesive carbon tape for imaging. Accelerating voltages, working distances, and magnification factors are indicated in-figure for each image.

3.6 X-RAY PHOTOELECTRON MICROSCOPY

Material samples were stored in an argon atmosphere glove box. Samples were removed from the glove box and pressed onto double-sided copper tape (3M Co.), in air, before being transferred into the XPS system. Care was taken to minimize exposure to air such that the total time between removal from the glove box until loading into the vacuum chamber of the XPS system was ≤ 40 minutes. Samples were left under ultra-high vacuum overnight before being transferred into the analysis chamber of the XPS, which had a base pressure of 10^{-10} mbar and was maintained below 2×10^{-9} mbar during the experiments. Analysis was performed with a SPECS spectrometer equipped with a Phoibos 150 hemispherical analyser, using unmonochromatized Mg Kα radiation, and a pass energy of 20 eV. Preliminary and final survey scans were compared to ensure that no photochemical degradation was induced during analysis. Data analysis was done using CasaXPS software (v. 2.3.18). Measured binding energies were adjusted to correct for the buildup of electrostatic charge by fitting the adventitious carbon peak and setting its center to 285.0 eV.

3.7 SOLID-STATE NUCLEAR MAGNETIC RESONANCE SPECTROSCOPY

The 27Al magic angle spinning (MAS) solid-state NMR spectra were acquired on a Bruker Avance (16.4 T) spectrometer with Larmor frequency of 182.46 MHz. The chemical shift scale was referenced externally to potassium alum, $KAl(SO_4)_2 \cdot 12H_2O$, at 0.033 ppm as the secondary reference. The spectra were acquired by excitation with a 1.2 μs pulse at 95 kHz rf field strength, adding 131,072 scans with 0.1 s delays. Samples were spun at 25.0 kHz about the magic angle, in rotors of 2.5 mm diameter. The final spectra

are shown after subtraction of the carefully phased and intensity adjusted signal (see Figure A.1) from the empty rotor and a spline baseline correction. Since this procedure does not give good results for the center region, where background and sample signals overlap, this region is disregarded for the analysis and blanked out for the overview plots in this work (Figure 5.3). Only the spinning sideband manifold, which does not overlap with background signal, is evaluated. Full spectra and the procedure are presented in the supplemental material (Figures A.1-A.2)

3.8 ELECTROCHEMICAL TESTING

All cells used in this thesis, both pouch cells and coin cells, were cycled under the same conditions. The electrolyte used was composed of 1 M $LiPF_6$ (Capchem, Shenzhen, China ≥ 99.9%) in a 1:1 solvent blend, by mass, of ethylene carbonate (EC, Capchem, < 20 ppm H_2O) and diethyl carbonate (DEC, Capchem, < 20 ppm H_2O). 1%, by mass, of the electrolyte additive $LiPO_2F_2$ (Capchem) was added to the solutions prior to cell construction/filling[10,11,12,13,14]. Cells were cycled in temperature-controlled boxes (30.0 ± 0.1°C) between 3.0 to 4.3 V using a Maccor 4000 Series automated test system (Maccor Inc., USA). Cells were cycled with either a C/5 formation cycle followed by C/3 cycling or a C/10 formation cycle followed by C/5 cycling. After cycling some of the coin cells were disassembled to check for electrode alignment issues to help explain observed testing behavior.

CHAPTER 4 FULL CELLS

In order to evaluate the performance of new positive electrode materials, they need to be made into LIBs for prolonged testing. Machine-made, commercially produced pouch cells provide very reproducible data, making them ideal for comparative electrolyte development and performance evaluations with fixed positive and negative electrode materials[58,59,60,61]. However, these cells are produced in large batches which require significant resources. It is therefore impractical to order an entire run of commercial cells to test every new possible electrode material. Rather, new materials are usually evaluated by constructing coin cells made with hand-made electrodes. Most research labs use half cells, with the new material as the positive electrode and a piece of lithium foil as the negative.

Half coin cells are relatively easy to make and can provide very repeatable data. Yet they can fail to accurately predict how a material would perform in an actual full cell. This is primarily because half cells have an abundance of lithium, which can mask problems with side reactions that use up available lithium. Thus, a half cell made with a certain positive electrode material might provide favorable results when in actuality a full cell made with the same material might perform poorly. Additionally, it is impossible to determine the effect of interactions between positive and negative electrodes that would result in a full Li-ion cell from data on half cells[62,63,]. In order to accurately predict the performance of new electrode materials in Li-ion batteries a method to make accurate and repeatable full coin cells would be valuable.

This chapter develops methods to prepare full coin cells, using graphite as the negative electrode material that allow for quality full coin cells with good reproducibility between cells to be made.

4.1 FABRICATING FULL COIN CELLS USING TRADITIONAL METHODS

The first step of this thesis was to build full coin cells following conventional half cell design. When preparing conventional half cells, a piece of Li metal foil is used as the negative electrode. The Li foil disk is usually larger than the working negative electrode or positive electrode. This allows for a much larger margin of error in alignment of electrode disks. However, when making full cells it is optimal to use positive and negative electrode disks with the same size[64]. Therefore, this work utilized positive and negative electrode disks with equal diameter. Otherwise, the initial design and assembly method was the same as for half coin cells. Many repeat full coin cells were made and taken for prolonged cycling tests in order to determine the reproducibility of full coin cells. The discharge capacity vs. cycle number is shown for three representative cells in Figure 4.1a. These cells were made with the configuration shown in Figure 3.1a, and cycled at C/3 with a C/5 formation cycle. Figure 4.1a shows that there was considerable variation between the cells. In order to consider the cause of this variance, these cells were moved into an argon-atmosphere glove box, taken apart, and photographed (Figure 4.1b). It was observed that the positive and negative electrodes were not exactly aligned in cells II and III, as indicated by the red circles in the figure, which outline the position of the positive electrode disks underneath the separators. This misalignment is shown clearly in the magnified images of cells II and III in Figure 4.1c.

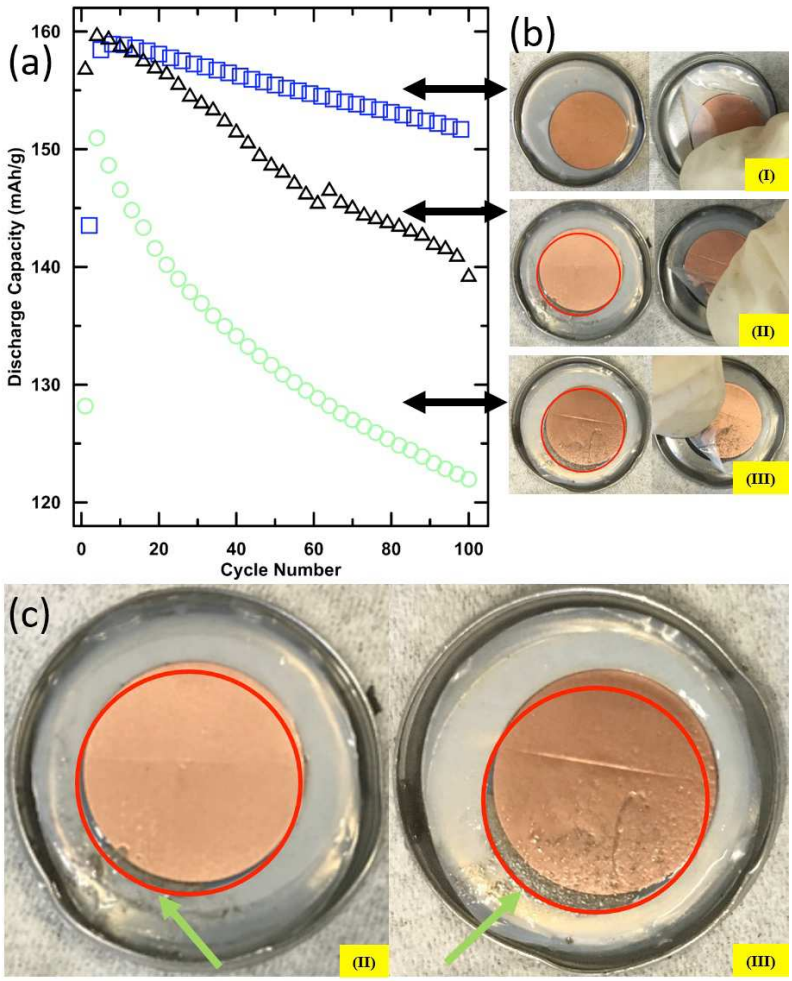

Figure 4.1: Three identical cells I, II, III (a) Discharge specific capacity vs. cycle number, (b) Photographs of disassembled cells with red circle showing position of positive electrode, (c) Magnified photos of cells II and III. The green arrows in (c) show evidence of Li plating where the positive electrode is not in alignment with the negative electrode. All cells were cycled at 30°C from 3 to 4.3 V at C/3 with a C/5 formation cycle.

It was further observed that lithium plating occurred in the areas where the positive electrode was not covered by the negative electrode. It is well-known that plating decreases the available lithium inventory and therefore reduces the available capacity of the cell[65,18]. The practical result is that of the three 'identical' cells shown in Figure 4.1, cell I retained ~95% of its initial capacity after 100 cycles, cell II retained ~90%, and cell III retained just ~80%. This capacity loss follows a direct relationship with the extent of the electrode

misalignment for these three cells. Considering the size of these electrode disks and that even a very minor misalignment can result in such significant performance losses, this assembly method is clearly unsuitable for comparative electrode material testing.

4.2 MISALIGNMENT IN TRADITIONAL FULL CELLS

The low precision of the first full coin cells is here attributed to electrode disk misalignment. It was therefore considered what causes this and how it may be mitigated or, ideally, prevented altogether. Following extensive trial and error, it was concluded that the misalignment occurs when the spring and spacer are placed on top of the electrode/separator stack. Typically, the assembly of such cells is performed using tweezers. When using this approach, the spring and spacer are held from one side, resulting in them being dropped from a slight angle. Even this small drop is enough to cause the misalignment that significantly decreased the cell performance of cells II and III in Figure 4.1. To prevent this problem several cells were made using the same construction but a vacuum pen was used to place the spring and spacer in the cell. The vacuum pen used can be seen in Figure 3.2. This simple modification of the method allowed the spring and spacer to be placed from directly above. In Figure 4.2 a significant improvement in cell performance can be seen between B cells (green diamonds) made with the use of a vacuum pen and A cells (black circles) made with the conventional construction. Additionally, for these B cells, cycling was slowed to C/10 for formation and C/5 for cycling to further reduce Li plating.

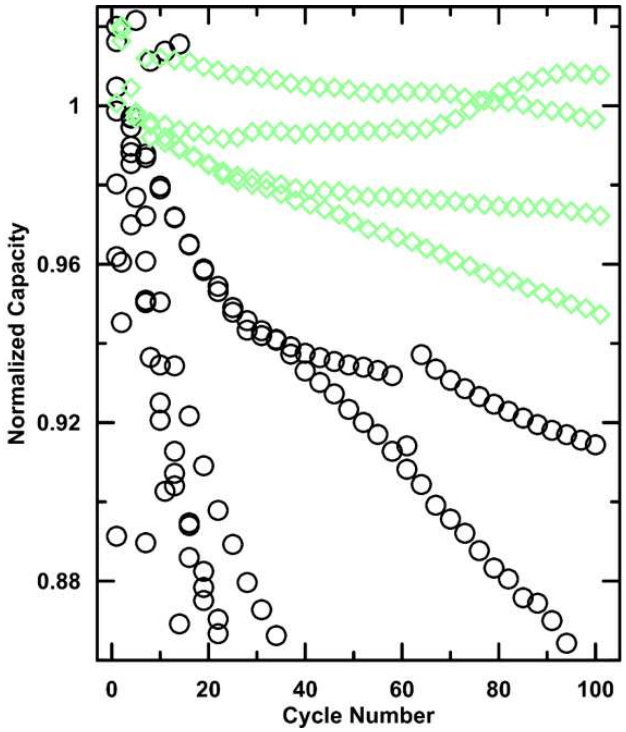

Figure 4.2: Normalized capacity vs. cycle cumber for cells of type A (black circles) using the standard method of coin cell fabrication and B (green diamonds) with the use of a vacuum pen. A cells were cycled at C/3 with a C/5 formation cycle. B cells were cycled at C/5 with a C/10 formation cycle. All cells were cycled at 30°C from 3 to 4.3 V.

4.3 EFFECT OF CHANGING SEPARATOR

Cells constructed with the aid of a vacuum pen showed significant improvements in performance and repeatability, however they were still not within the desired precision limits for high quality electrode material comparisons. It was next considered what role the use of two Celgard separators had. When a cell is crimped it becomes slightly curved. When this happens in a half cell, the pliable Li foil bends with the cell, maintaining contact and pressure throughout the cell. However, when making full cells the negative electrode disk is not as compliant and so it was considered whether there was uneven pressure throughout the cell. BMF separators are thicker and more compressible than Celgard separators, which was hypothesized to help more evenly maintain pressure in full coin

cells. Figure 4.3 shows a comparison of repeat cells using either two Celgard separators versus one BMF separator. The results show that the use of a single BMF separator significantly increased the reproducibility of triplicate full coin cells (Figure 4.3b).

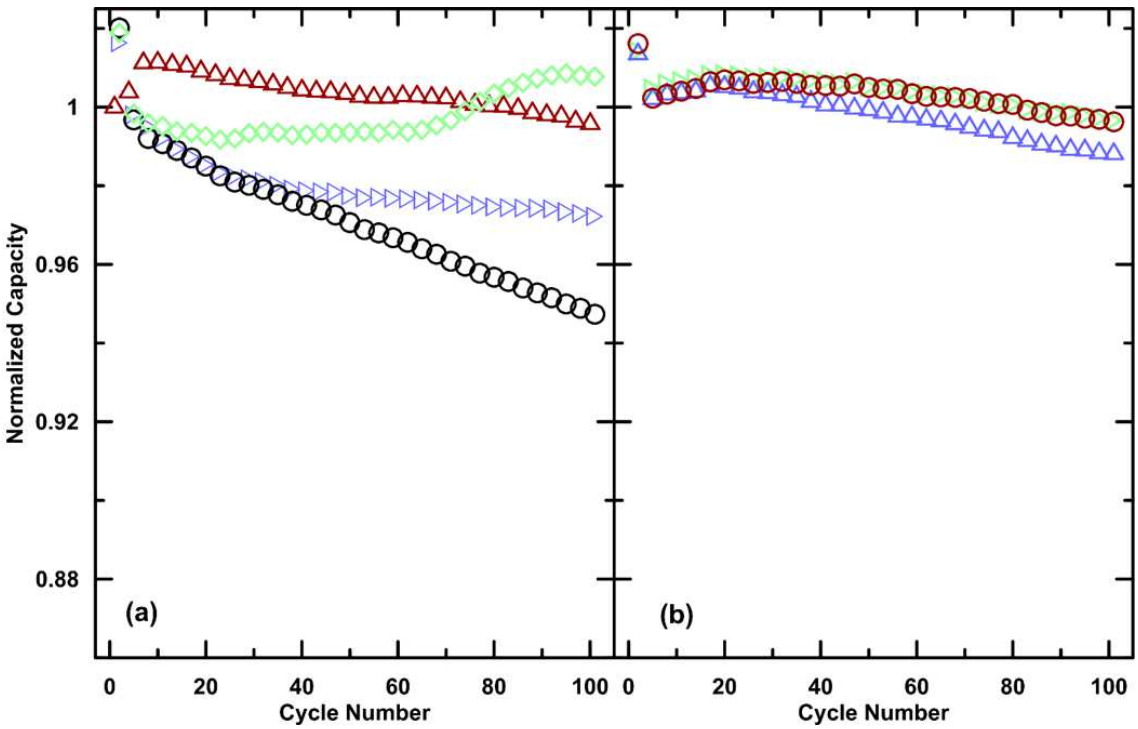

Figure 4.3: (a) Cells made with two Celgard separators, compared to (b) cells made with one BMF separator. Cells were cycled at 30°C from 3 to 4.3 V at C/5 with a C/10 formation cycle.

4.4 COMPARING FULL COIN CELLS WITH COMMERCIALLY PRODUCED POUCH CELLS

Finally, the cycling behavior of full coin cells that were prepared with electrodes of equal diameter, a single BMF separator, and assembled using a vacuum pen (Figure 4.4b) was compared to the performance of machine-made pouch cells (Figure 4.4a). Cells were prepared with the same electrolyte and under identical conditions. For both cell types there are two datasets: i) Electrochemical tests performed in winter that were stopped after 100

cycles (A, C) and ii) electrochemical tests performed in summer and stopped after 200 cycles (B, D). This second set of testing was performed in summer when the outside temperature rose such that the temperature-controlled environments rose slightly above the 30°C set point. These temperature variations are seen in the data, further demonstrating the importance of controlling every aspect of these experiments. Nonetheless, the results show that the full coin cells have dramatically superior precision than the first batch, which was shown in Figure 4.1. The reproducibility of these cells is here proposed to be sufficient for comparative materials testing, with the significant advantages over conventional half coin cell designs.

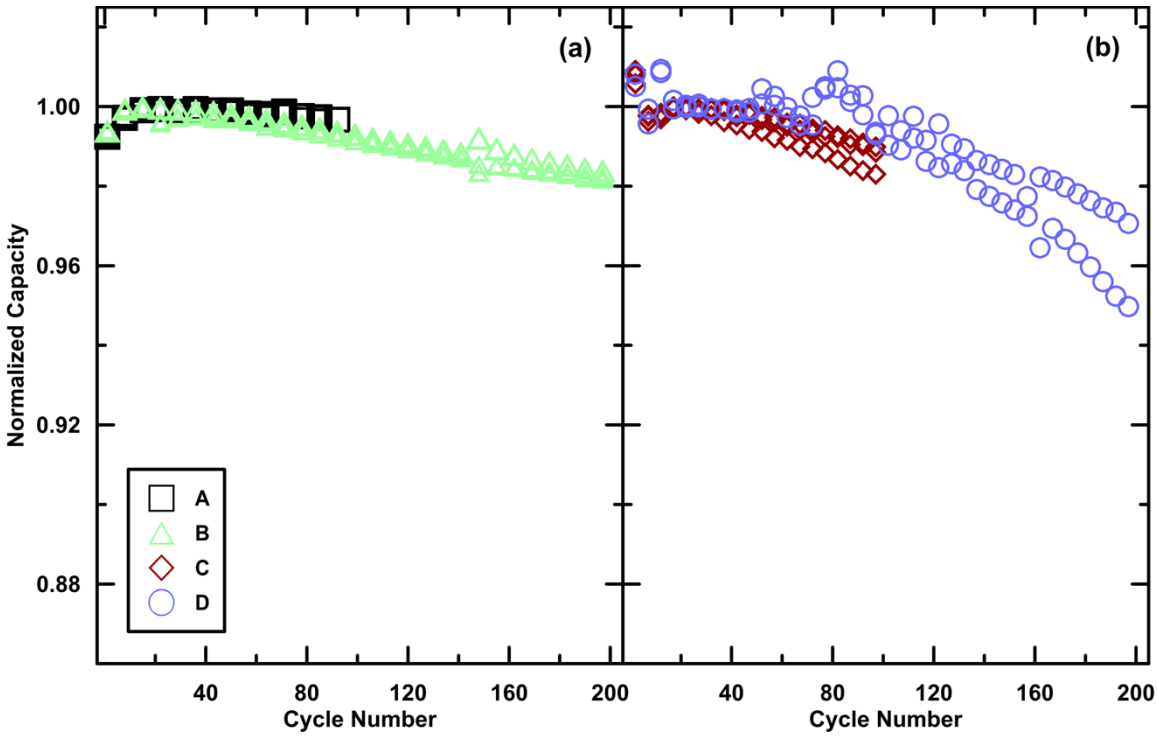

Figure 4.4: NMC 622A/Graphite cells (a) pouch cells, (b) full coin cells. A and C represent repeats of pouch and full coin cells respectively that were cycled during the winter for 100 cycles. B represents repeats of pouch cells that were cycled during the fall and D represents repeats of full coin cells that were cycled during the summer. B and D were cycled for 200 cycles. All cells were cycled at 30°C from 3 to 4.3 V at C/5 with a C/10 formation cycle.

4.5 USING FULL COIN CELLS TO STUDY POSITIVE ELECTRODE MATERIALS

The results of the study into how to make reliable, reproducible full coin cells indicate that while it is slightly more challenging than full coin cells, with care they can be made to a satisfying degree. The next chapter, Chapter 5, will use this method to evaluate the ALD Al_2O_3 coatings on both NMC and NCA positive electrode materials.

CHAPTER 5 COATINGS

This chapter will examine what happens to ALD Al_2O_3 coatings on both $LiNi_{0.6}Mn_{0.2}Co_{0.2}O_2$ (NMC622) and $LiNi_{0.8}Co_{0.15}Al_{0.5}O_2$ (NCA8155) during annealing to various temperatures and how this affects the electrochemical performance of full coin cells. The effects of heat treatment are examined for samples annealed in the temperature range of 400°C to 900°C, as well as the effect of two coating thicknesses. The results from both characterization and electrochemical testing will be presented. This chapter summarizes work in the article: "Diffusion of Al^{3+} ions from Atomic Layer Deposited Al_2O_3 Surface Coatings into Positive Electrode Materials and the Effects Thereof" by Vivian Murray, David Hall, Leah Ellis, Ulrike Werner-Zwanziger, Jing Li, I.G. Hill, and J.R. Dahn which has been submitted to Tesla for approval for publication. VM made the samples, assisted with data collection and wrote parts of the manuscript of the paper. Leah Ellis did the XPS measurements and assisted with data analysis. Ulli Werner-Zwanziger did the ssNMR measurements and assisted with their interpretation. David Hall and Jeff Dahn assisted with interpretation of data, experiment design and editing the manuscript.

5.1 MATERIAL CHARACTERIZATION

5.1.1 Scanning Electron Microscopy

Figure 5.1 shows SEM images of the NCA materials. In Figures 5.1a and 5.1b, the pristine material has clean, smooth surfaces with good crystallinity. Figures 5.1c, 5.1d, 5.1e, and 5.1f show SEM images of the NCA sample with the thin coating and no heat treatment, and after annealing to 600°C, respectively. These images indicate a dense coating. The pattern visible in Figures 5.1c, 5.1d, 5.1e and 5.1f possibly indicates the

coating is not entirely uniform. In Figures 5.1g and 5.1h, after being annealed to 900°C, the sample shows no evidence of coating, suggesting all of the coating has been diffused into the bulk electrode material.

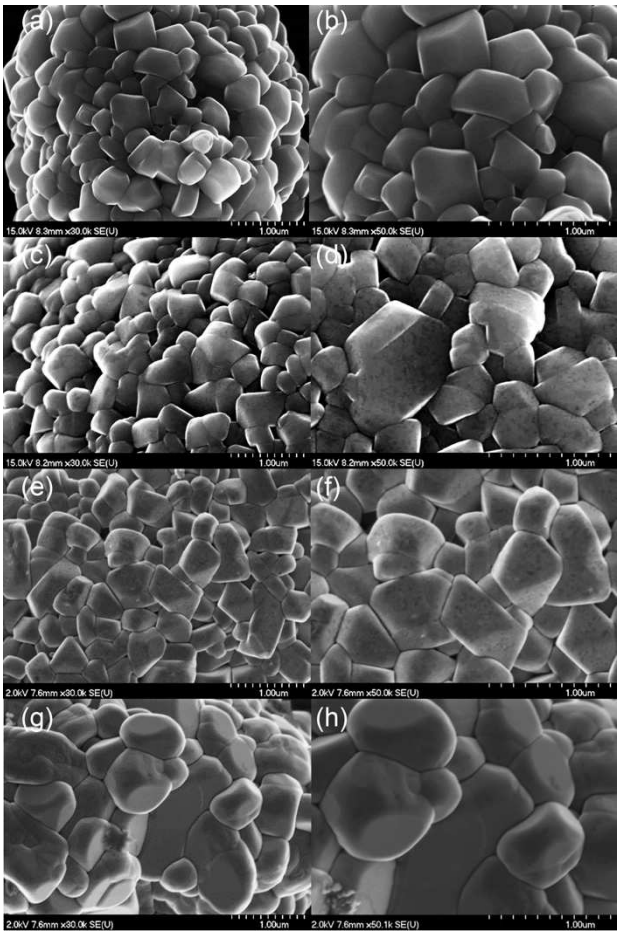

Figure 5.1: SEM images of (a, b) Pristine NCA801505, (c, d) NCA801505 Thin Coating, No Heat, (e, f) NCA801505 Thin Coating, 500°C, (g, h) NCA801505 Thin Coating, 900°C.

Figure 5.2 shows the SEM images of the NMC materials, which follow a similar pattern to those of the NCA. The SEM reveals a dense coating and after being annealed to 900°C there is no more evidence of a coating, again suggesting the coating has entirely diffused into the bulk.

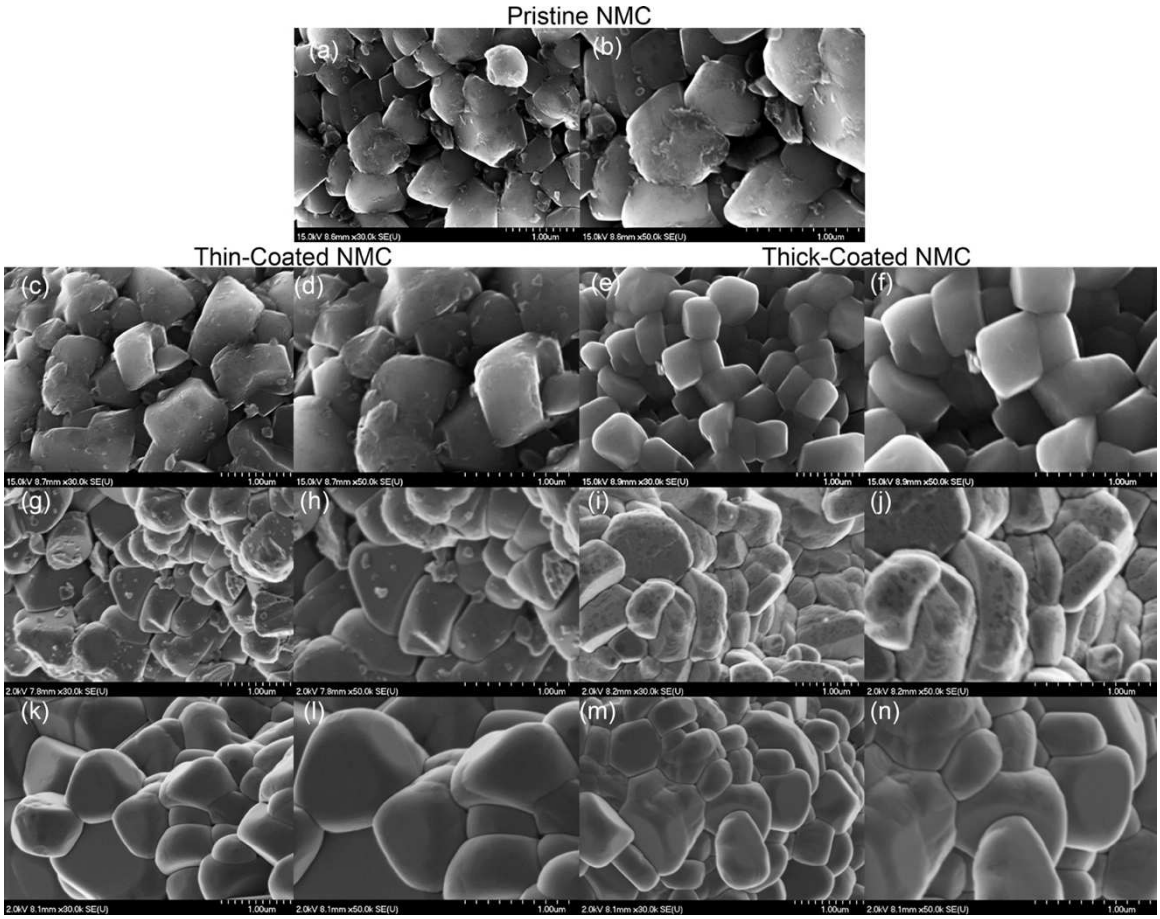

Figure 5.2: SEM images of (a, b) Pristine NMC622, (c, d) NMC622 Thin Coating, No Heat, (g, h) NMC622 Thin Coating, 500°C, (k, l) NMC622 Thin Coating, 900°C, (e, f) NMC622 Thick Coating, No Heat, (i, j) NMC622 Thick Coating, 500°C, (m, n) NMC622 Thick Coating, 900°

5.1.2 Solid State Nuclear Magnetic Resonance Spectroscopy

Due to the ultrathin nature of ALD coating, even with the thicker coating on the two samples, the limited amount of Al present in the coating made it challenging to detect a signal using ^{27}Al ssNMR. A rotor synchronized Hahn-echo sequence was used by Han et al.[39] to study the local ^{27}Al environments in thicker Al_2O_3 coatings on NMC materials. Unfortunately, Hahn-echo excitation using various conditions did not produce sufficient

^{27}Al NMR signal intensity in a reasonable amount of time for this approach to be useful for our samples. Ultimately, the samples were analyzed using excitation with a single pulse, whose lengths were optimized to maximize the signals of 4-fold and 6-fold coordinated ^{27}Al sites in Al_2O_3 to provide the greatest signal-to-noise ratio for our samples. An attempt was made to remove the probe background signal via post-measurement subtraction of the spectrum acquired under similar conditions on an empty rotor, as illustrated in Figure A.2. While in general for sufficiently concentrated diamagnetic samples this procedure is successful, the samples studied here pose two problems: Firstly, these samples give a different electronic response to the probe tuning and matching, due to their paramagnetic character, thereby preventing a characterization of the background signal under "identical" conditions. Secondly, the intensity of the background signal from the static parts of the probe head is significantly larger than the signal of the samples. Ultimately, we exploit the fact that the ^{27}Al NMR background spectrum does not contain sharp spinning sidebands, in contrast to the spectra of the samples spinning at 25 kHz. So, although the center peak is too distorted to be useful, by comparing the intensities of the spinning sideband manifolds to the pristine sample, the relative amount of coating present after each heat treatment may be determined (Figure 5.3).

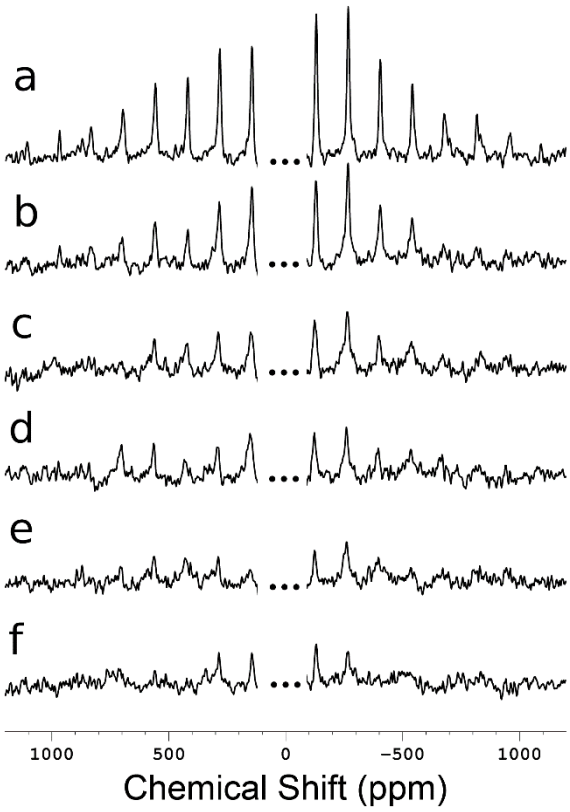

Figure 5.3: Comparison of the 27Al NMR spinning side- band manifolds of samples of thick coated NMC622 samples with (a) No heat treatment (b) 400°C (c) 500°C (d) 600°C (e) 700°C (f) 900°C.

The ^{27}Al ssNMR spectra demonstrate that as the annealing temperature is increased, the relative intensity of the sharp spinning sideband signal decreases, indicating that the aluminum nuclei leave the well-structured Al_2O_3 coating environment. Most likely the aluminum diffuses into the NMC core during heating. While ^{27}Al ssNMR signals have been observed within NCA related materials[66,67], the magnetic properties of the core NMC material would cause heavily Knight-shifted and broadened ^{27}Al NMR signals. These require Hahn- or solid-echo techniques together with excitation frequency stepping for detection and cannot be observed with the technique applied here. As the annealing temperature is increased, the amount of diffusion that occurred also increased, leading to

greater relative NMR signal intensity loss. Given that the materials were all annealed for the same amount of time, it can be concluded that the temperature affects the diffusion rate. At first, these findings appear contradictory to those of Han et al., who observe 4-fold coordinated ^{27}Al sites at around 69 ppm following heat treatment, which they assign to $LiAlO_2$[39]. However, this may be explained by the thickness of the Al_2O_3 coatings. Han et al., report the Al_2O_3 content was ~2 wt. %, which is an order of magnitude greater than the ALD-coated NMC in the present work (approx. 0.2%). It is therefore reasonable that a significant amount of $LiAlO_2$ can be formed under their conditions. For our samples, especially the one heated to 400°C (Figure 3b), the ^{27}Al ssNMR spectra may contain spinning sidebands corresponding to $LiAlO_2$ signals, but their intensities fall within the noise level. Zhou et al. have clearly shown that Al can be incorporated within the structure of NMC so it is natural to expect interdiffusion and little, if any $LiAlO_2$ formation in our samples[68].

5.1.3 X-Ray Photoelectron Microscopy

Figure 5.4 shows the results of XPS on the NMC samples. The Al 2p peak appears at 74.1 eV, as expected for Al_2O_3[69]. The area under the peaks reflect the amount of Al_2O_3 coating present within each sample. In Figure 5.4a, in the NMC thick samples, this remains relatively constant following annealing up to 600°C. For the sample that was annealed at 700°C, the Al 2p peak intensity is noticeably decreased. The Al 2p peak intensity shows a further decrease in the sample heated to 800°C and is no longer present in the XPS spectrum collected from the sample annealed at 900°C. Rather, the spectrum resembles that of the pristine (i.e., uncoated) material. The relative intensity of Al peaks discussed are based on

peak area calculations. These results are generally consistent with the ssNMR finding that during annealing, Al diffuses into the NMC material. However, the onset temperature is apparently different (discussed further below). A similar trend can be seen for the thin-coated NMC material (Figure 5.4b), however the Al 2p peak intensity begins to decrease after only 600°C.

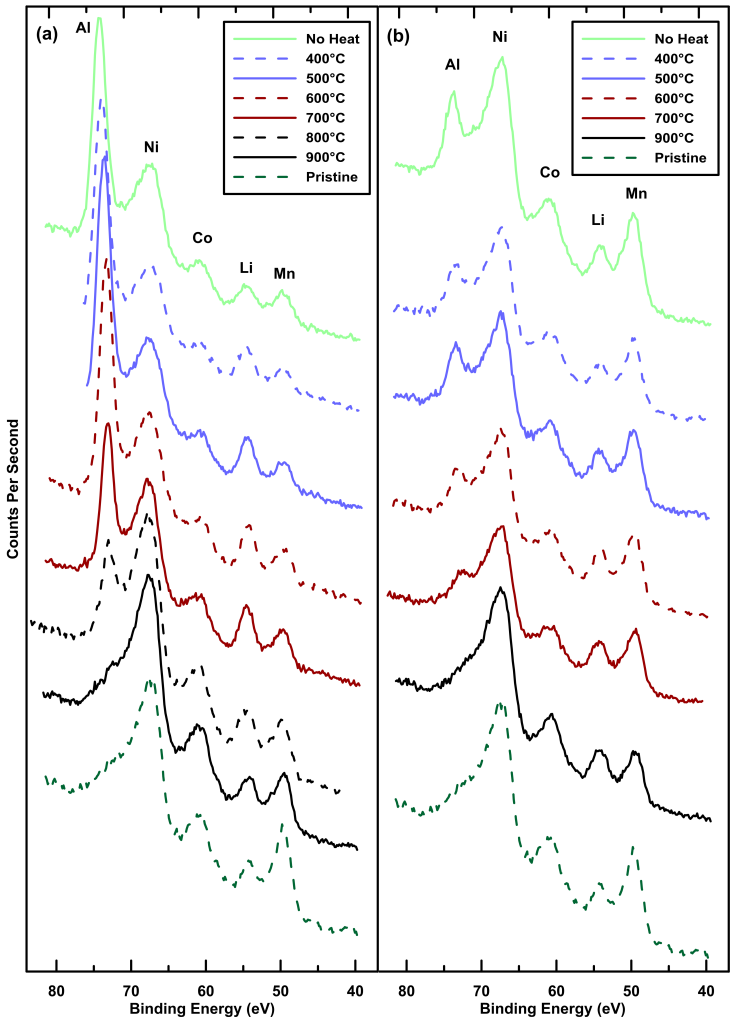

Figure 5.4: XPS results of NMC622 samples of (a) thick coated and (b) thin coated. Al peak decreases with heat treatment after 700°C for the thick coating and 600°C for the thin coating.

Figure 5.5 shows XPS analysis of the NCA samples. Both thick and thin Al_2O_3-coated samples follow the same trend as the NMC materials (Figure 5.4), with the NCA thick samples (Figure 5.5a) showing a decrease in the Al peak intensity after annealing at 700°C and the thin samples (Figure 5.5b) after annealing at 600°C.

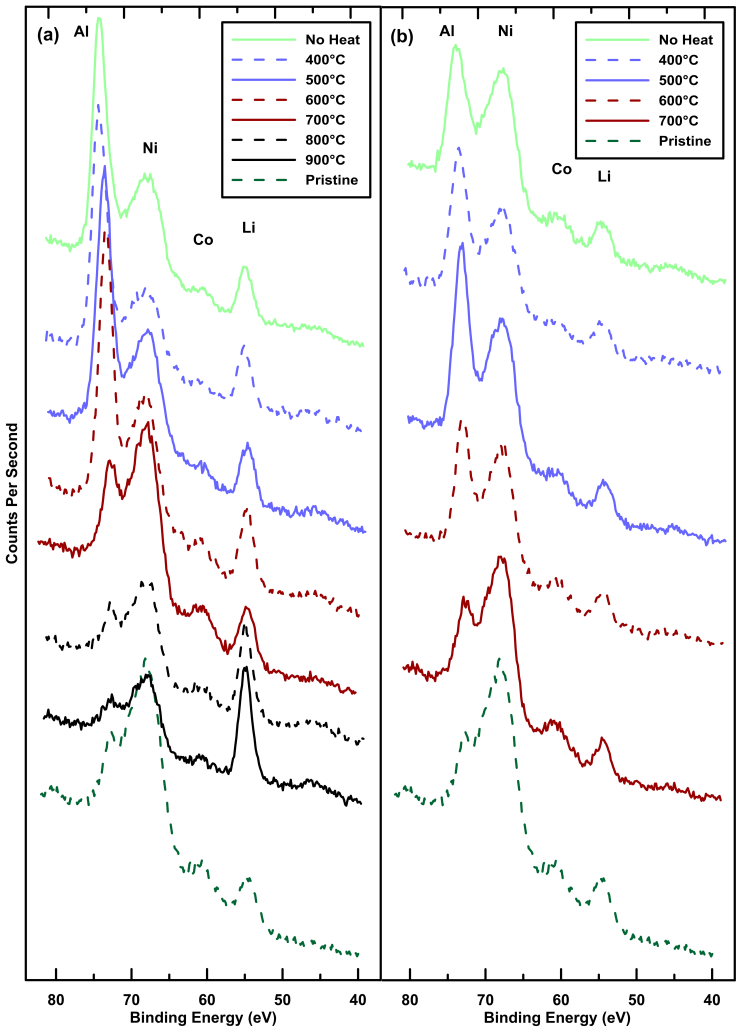

Figure 5.5: XPS results of NCA801505 samples of (a) thick coated and (b) thin coated. Al peak decreases with heat treatment after 700°C for the thick coating and 600°C for the thin coating.

5.2 CHARACTERIZATION SUMMARY

The results of the XPS and ^{27}Al MAS ssNMR on the NMC samples are summarized in Figure 5.6. Here the amount of Al_2O_3 coating present in each sample after being heat treated is calculated relative to the amount present in the unheated sample. From these results the following models are proposed. In Figure 5.7a diffusion of the thicker Al_2O_3 coating into the NMC particle is shown. In the diagram the NMC particle is shown in the center in blue. The coating is shown outside in green. As the coating begins to diffuse into the NMC particle, the interdiffusion region is shown in beige. Figure 5.7b depicts the proposed diffusion of the thinner coating. It is important to note that ssNMR measures signal from the entire material, provided the signal is not suppressed by magnetic effects (as is proposed for ^{27}Al that has diffused into the NMC core material). In contrast, the depth of analysis of XPS measurements are limited to the very surface of a sample, according to the inelastic mean free path of the photoelectrons[70,71]. For this reason, the approximate depth of the XPS measurements is depicted in Figure 5.7. This important distinction between the two techniques fully rationalizes the differences in the relative intensity losses summarized in Figure 5.6. Due to the Al_2O_3 coatings being thicker than the measurement depth of XPS, samples must be annealed to 600°C and 700°C for the thin coating and thick coatings, respectively, before the diffusion is observable by XPS. Because ssNMR is not limited to surface measurement, the diffusion is detected immediately, which in these materials is following annealing at just 400°C.

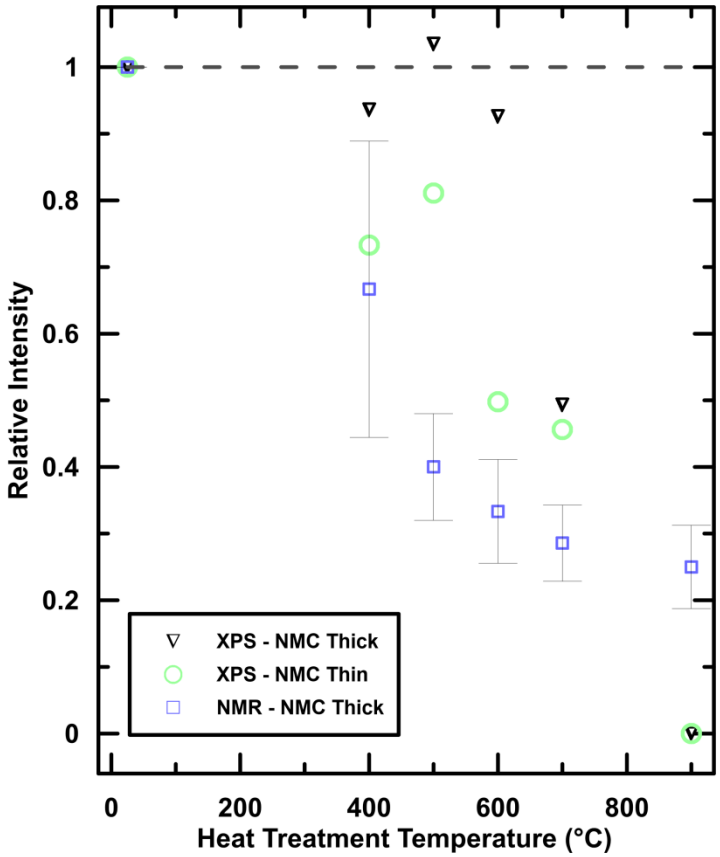

Figure 5.6: Intensity of Al peak present after being annealed relative to as-coated sample of NMC622 samples as measured by XPS for thick coating (black triangle) and thin coating (green circle) or by 27Al NMR of thick coating (blue square).

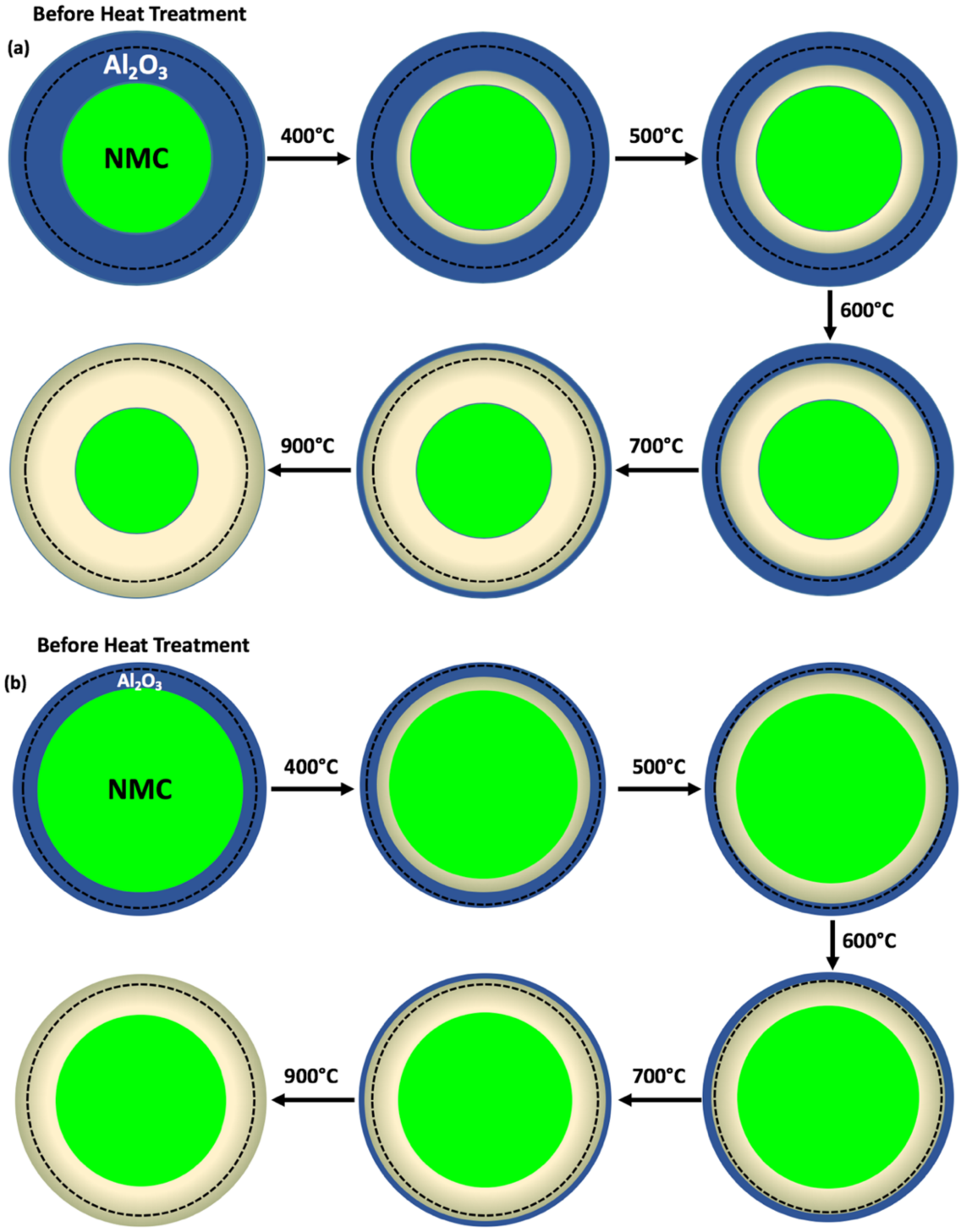

Figure 5.7: Schematic of Al_2O_3 coating on NMC622 particle and effect of heat treatment with (a) thick coating or (b) thin coating.

5.3 ELECTROCHEMICAL TESTING RESULTS

Electrochemical testing was performed using full coin cells on selected samples of the thicker coated NMC and NCA. For the NMC, full cells were made from (i) the pristine material, (ii) coating with no heat treatment, (iii) coating annealed to 600°C and (iv) coated annealed to 900°C. NCA full cells were also made from the (i) pristine material, (ii) coating with no heat treatment, and (iii) coating annealed to 600°C. However, a problem was encountered during attempts to make electrodes from the material annealed at 900°C. When this sample was added to the slurry mixture to make electrodes the resulting slurry was not suitable to make electrodes. The slurry was much more viscous than normal and the resultant electrode was flaky and unusable. Several attempts were made with altering the slurry recipe with no improvement. The same problem was encountered with the sample annealed to 800°C so the sample annealed to 700°C was used as the upper limit.

In Figure 5.8a, the results of cycling of full coin cells made from the NCA materials are shown. The coated, 700°C cells perform the worst and close behind them are the cells made from coated materials that were not annealed. The pristine, uncoated material performed the best and the coated 600°C cells performed similarly. This is in contrast to numerous literature reports that show that ALD coated materials outperform uncoated materials[41,43,50,72,73]. This may mean that in the presence of the highly effective $LiPO_2F_2$ electrolyte additive that the impact of the coating is minimal[74,75].

In Figure 5.8b, there is a similar trend in the cells made from NMC materials. However, none of the full cells made from Forge Nano materials perform comparably to the full coin cells shown in Figure 5.8c. These cells were made from positive and negative electrodes punched from the commercial NMC622A/graphite pouch cells and cycled under

the same conditions. The superior performance of the cells made from commercial electrodes may be due to the possible superior quality of the commercial electrodes compared to the electrodes made at Dalhousie University.

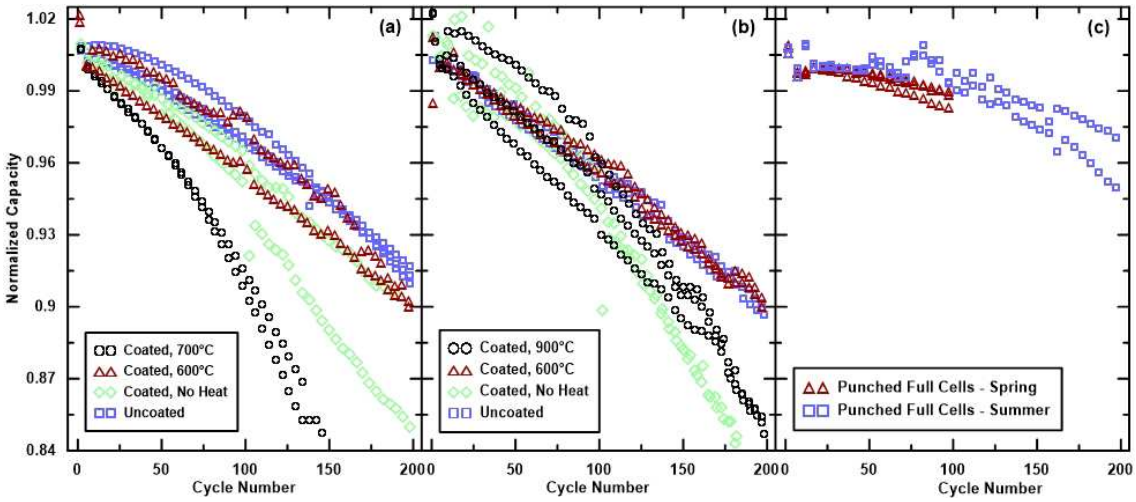

Figure 5.8: Normalized capacity vs. cycle number (a) full coin cells made from NCA801505 pristine, as-coated or coated and annealed as the positive and artificial graphite for the negative, (b) full coin cells made from NMC622 pristine, as-coated or coated and annealed as the positive and artificial graphite for the negative and (c) Full coin cells made with electrodes punched from commercial NMC622A/graphite pouch cells for comparison. All cells were cycled at 30°C between 3.0 to 4.3 V using Maccor cyclers at C/5 with a C/10 formation cycle. For each material at least two repeats of each cell were made.

CHAPTER 6 CONCLUSIONS

6.1 Concluding Remarks

The development of new positive electrode materials is important in LIB research to improve energy density and increase lifetime of batteries. Chapter 4 of this work demonstrates methods for the construction of full NMC/graphite coin cells. By constructing cells with positive and negative electrodes of equal diameter, with a single BMF separator (rather than two thinner Celgard separators), and constructing the cells with a vacuum pen (rather than tweezers), coin cells were built with suitable precision for comparative electrode materials testing. Full coin cells have the significant advantage of more accurately representing the relative performance of new materials in actual lithium-ion cells than conventional half coin cell constructions. The results of this work will benefit the development and evaluation of new positive electrode materials. These methods were used in Chapter 5.3 of this work, to compare the electrochemical performance of the positive electrode materials studied.

In Chapter 5 of this work, ALD Al_2O_3-coated NMC and NCA materials were annealed at temperatures in the range 400 – 900°C and characterized by ^{27}Al ssNMR and XPS. The results demonstrate Al diffusion into the core electrode material at a temperature-dependent rate. Differences between the ssNMR and XPS results are explained by the limited depth of analysis of XPS and the results were used to make a schematic of surface-coating diffusion.

As expected from Al_2O_3-coated materials that are prepared using conventional wet chemical methods, heating ALD-coated materials is important for electrochemical performance. The results indicate that 600°C is ideal for the thicker coated materials

examined in this work. For both the NCA and NMC materials the 600°C heated material performs as well as the uncoated material however none of the materials perform as well as the coin cells made from commercial NMC622A electrodes extracted from the pouch cells. It is important to note that all the electrolytes used in this work contained 1% by weight of $LiPO_2F_2$, a highly effective electrolyte additive, which may render the impact of coatings to be minimal, compared to electrolytes with no additives or conventional additives like vinylene carbonate.

6.2 Future Work

The method of fabricating full coin cells presented in this work could be a very useful approach for academic researchers. However while the performance of coin cells made with electrodes punched from pouch cells was compared to the performance of pouch cells, no experimentation was done to look at the performance of handmade electrodes. In order to use this method to directly compare new positive electrode materials against commercially made cells, the quality and performance of handmade electrodes should be studied. This could be accomplished by fabricating full coin cells made with handmade electrodes of the same composition as those found in pouch cells and cycling both for comparison. This would verify the quality of the handmade electrodes.

Many previous works have been published showing the benefit of an Al_2O_3 coating on positive electrode performance[33,34,35,36,39,41,43]. To investigate whether the impact of the additive $LiPO_2F_2$ can negate the benefits of the coating, these previous studies should be redone with $LiPO_2F_2$ as an additive to determine if this changes the results showing the benefit of the coating.

In the paper by Han et al.[45], full coin cells were used to study the effect of an Al_2O_3 coating on NMC. The testing protocol used in this paper was more rigorous than the one used in the current work. Han et al. cycled their full coin cells between 3 and 4.4V at C/10 for 4 cycles and then C/3 for 100 cycles. Unlike in the current work however Han et al. held their cells at 4.4V for 3 hours after each cycle. Their work shows an improvement in the cycling performance for the coated materials that grow with each cycle. It is possible that when using full coin cells, in order to see the benefit of the coating a more rigorous cycling protocol must be used.

Due to time limitations only some of the materials used in this project were made into full coin cells for electrochemical testing. Previous research has suggested that thinner Al_2O_3 coatings perform better than thicker coatings[35,38,39,43]. Only the thicker coated materials were tested in this work but the effect of the thickness of the coating should also be evaluated. The electrochemical testing should be performed with the thinner coatings as well.

REFERENCES

1. W. Li, B. Song, and A. Manthiram, *Chem. Soc. Rev.*, **46**, 3006–3059 (2017).

2. N. Nitta, F. Wu, J. T. Lee, and G. Yushin, *Materials Today*, **18**, 252–264 (2015).

3. Z. Wu, S. Ji, J. Zheng, Z. Hu, S. Xiao, Y. Wei, Z. Zhuo, Y. Lin, W. Yang, K. Xu, K. Amine, and F. Pan, *Nano Letters*, **15**, 5590–5596 (2015).

4. F. Zhou, X. Zhao, A. J. Smith, and J. R. Dahn, *J. Electrochem. Soc.*, **157**, A399–A406 (2010).

5. Y. Wei, J. Zheng, S. Cui, X. Song, Y. Su, W. Deng, Z. Wu, X. Wang, W. Wang, M. Rao, Y. Lin, C. Wang, K. Amine, and F. Pan, *J. Am. Chem. Soc.*, **137**, 8364–8367 (2015).

6. Y.-K. Sun, S.-W. Cho, S.-W. Lee, C. S. Yoon, and K. Amine, *J. Electrochem. Soc.*, **154**, A168–A172 (2007).

7. J. Dahn and G. M. Ehrlich, in *Linden's Handbook of Batteries*,, McGraw-Hill, New York (2011).

8. T. Marks, S. Trussler, A. J. Smith, D. Xiong, and J. R. Dahn, *J. Electrochem. Soc.*, **158**, A51–A57 (2011).

9. C. Pillot, The Rechargeable Battery Market and Main Trends 2016-2025. Presented at the 33rd Annual International Battery Seminar and Exhibit, Fort Lauderdale, USA 2016.

10. G. E. Blomgren, *J. Electrochem. Soc.*, **164**, A5019–A5025 (2017).

11. A. K. March 2018, *Chemistry World* https://www.chemistryworld.com/news/battery-builders-get-the-cobalt-blues/3008738.article. (accessed on December 14, 2018)

12. M. Wissler, *Journal of Power Sources*, **156**, 142–150 (2006).

13. T. Zheng, J. N. Reimers, and J. R. Dahn, *Physical Review B*, **51**, 734–741 (1995).

14. J. R. Dahn, T. Zheng, Y. Liu, and J. S. Xue, *Science*, **270**, 590–593 (1995).

15. K. Xu, *Chemical Reviews*, **104**, 4303–4418 (2004).

16. S. J. An, J. Li, C. Daniel, D. Mohanty, S. Nagpure, and D. L. Wood, *Carbon*, **105**, 52–76 (2016).

17. A. J. Smith, J. C. Burns, X. Zhao, D. Xiong, and J. R. Dahn, *J. Electrochem. Soc.*, **158**, A447–A452 (2011).

18. A. J. Smith, J. C. Burns, D. Xiong, and J. R. Dahn, *J. Electrochem. Soc.*, **158**, A1136–A1142 (2011).

19. J. A. Gilbert, I. A. Shkrob, and D. P. Abraham, *J. Electrochem. Soc.*, **164**, A389–A399 (2017).

20. L. M. Thompson, W. Stone, A. Eldesoky, N. K. Smith, C. R. M. McFarlane, J. S. Kim, M. B. Johnson, R. Petibon, and J. R. Dahn, *J. Electrochem. Soc.*, **165**, A2732–A2740 (2018).

21. C. Zhan, T. Wu, J. Lu, and K. Amine, *Energy & Environmental Science*, **11**, 243–257 (2018).

22. S.-K. Jung, H. Gwon, J. Hong, K.-Y. Park, D.-H. Seo, H. Kim, J. Hyun, W. Yang, and K. Kang, *Advanced Energy Materials*, **4**, 1300787 (2014).

23. F. Schipper, E. M. Erickson, C. Erk, J.-Y. Shin, F. F. Chesneau, and D. Aurbach, *J. Electrochem. Soc.*, **164**, A6220–A6228 (2017).

24. D. J. Xiong, L. D. Ellis, J. Li, H. Li, T. Hynes, J. P. Allen, J. Xia, D. S. Hall, I. G. Hill, and J. R. Dahn, *J. Electrochem. Soc.*, **164**, A3025–A3037 (2017).

25. M. Hirayama, K. Sakamoto, T. Hiraide, D. Mori, A. Yamada, R. Kanno, N. Sonoyama, K. Tamura, and J. Mizuki, *Electrochimica Acta*, **53**, 871–881 (2007).

26. J. Li, L. E. Downie, L. Ma, W. Qiu, and J. R. Dahn, *J. Electrochem. Soc.*, **162**, A1401–A1408 (2015).

27. Z. Wang, C. Wu, L. Liu, F. Wu, L. Chen, and X. Huang, *J. Electrochem. Soc.*, **149**, A466–A471 (2002).

28. Y. Chen, Y. Zhang, B. Chen, Z. Wang, and C. Lu, *Journal of Power Sources*, **256**, 20–27 (2014).

29. Z. Zhang, Z. Gong, and Y. Yang, *J. Phys. Chem. B*, **108**, 17546–17552 (2004).

30. G. T.-K. Fey, H.-Z. Yang, T. Prem Kumar, S. P. Naik, A. S. T. Chiang, D.-C. Lee, and J.-R. Lin, *Journal of Power Sources*, **132**, 172–180 (2004).

31. W. Cho, S.-M. Kim, J. H. Song, T. Yim, S.-G. Woo, K.-W. Lee, J.-S. Kim, and Y.-J. Kim, *Journal of Power Sources*, **282**, 45–50 (2015).

32. D. Wang, X. Li, Z. Wang, H. Guo, Z. Huang, L. Kong, and J. Ru, *Journal of Alloys and Compounds*, **647**, 612–619 (2015).

33. J. Cho, Y. J. Kim, and B. Park, *Chemistry of Materials*, **12**, 3788–3791 (2000).

34. L. Liu, *Solid State Ionics*, **152–153**, 341–346 (2002).

35. K. J. Cao, L. Wang, L. C. Li, and G. C. Liang, *Applied Mechanics and Materials* (2013) https://www.scientific.net/AMM.320.235.

36. A. M. Kannan, L. Rabenberg, and A. Manthiram, *Electrochem. Solid-State Lett.*, **6**, A16–A18 (2003).

37. J.-Y. Liao and A. Manthiram, *Journal of Power Sources*, **282**, 429–436 (2015).

38. S.-T. Myung, K. Izumi, S. Komaba, Y.-K. Sun, H. Yashiro, and N. Kumagai, *Chem. Mater.*, **17**, 3695–3704 (2005).

39. B. Han, T. Paulauskas, B. Key, C. Peebles, J. S. Park, R. F. Klie, J. T. Vaughey, and F. Dogan, *ACS Applied Materials & Interfaces*, **9**, 14769–14778 (2017).

40. B. Han, B. Key, S. H. Lapidus, J. C. Garcia, H. Iddir, J. T. Vaughey, and F. Dogan, *ACS Appl. Mater. Interfaces*, **9**, 41291–41302 (2017).

41. Y. Shi, M. Zhang, D. Qian, and Y. S. Meng, *Electrochimica Acta*, **203**, 154–161 (2016).

42. S. M. George, *Chemical Reviews*, **110**, 111–131 (2010).

43. L. A. Riley, S. Van Atta, A. S. Cavanagh, Y. Yan, S. M. George, P. Liu, A. C. Dillon, and S.-H. Lee, *Journal of Power Sources*, **196**, 3317–3324 (2011).

44. L. Zheng, T. D. Hatchard, and M. N. Obrovac, *MRS Communications*, 1–6 (2018).

45. B. Han, A. R. Dunlop, S. E. Trask, B. Key, J. T. Vaughey, and F. Dogan, *J. Electrochem. Soc.*, **165**, A3275–A3283 (2018).

46. Y. Su, S. Cui, Z. Zhuo, W. Yang, X. Wang, and F. Pan, *ACS Appl. Mater. Interfaces*, **7**, 25105–25112 (2015).

47. T. Feng, Y. Xu, Z. Zhang, X. Du, X. Sun, L. Xiong, R. Rodriguez, and R. Holze, *ACS Appl. Mater. Interfaces*, **8**, 6512–6519 (2016).

48. R. W. Johnson, A. Hultqvist, and S. F. Bent, *Materials Today*, **17**, 236–246 (2014).

49. Y. S. Jung, A. S. Cavanagh, Y. Yan, S. M. George, and A. Manthiram, *J. Electrochem. Soc.*, **158**, A1298–A1302 (2011).

50. Y.-S. Jung, A. S. Cavanagh, A. C. Dillon, M. D. Groner, S. M. George, and S.-H. Lee, *Journal of the Korean Ceramic Society*, **47**, 61–65 (2010).

51. A. W. Ott, J. W. Klaus, J. M. Johnson, and S. M. George, *Thin Solid Films*, **292**, 135–144 (1997).

52. M. D. Groner, F. H. Fabreguette, J. W. Elam, and S. M. George, *Chemistry of Materials*, **16**, 639–645 (2004).

53. A. C. Dillon, A. W. Ott, J. D. Way, and S. M. George, *Surface Science*, **322**, 230–242 (1995).

54. C. Chi, H. Katsui, R. Tu, and T. Goto, *Materials Chemistry and Physics*, **143**, 1338–1343 (2014).

55. J. Li, S. L. Glazier, K. Nelson, X. Ma, J. Harlow, J. Paulsen, and J. R. Dahn, *J. Electrochem. Soc.*, **165**, A3195–A3204 (2018).

56. L. D. Ellis, J. P. Allen, I. G. Hill, and J. R. Dahn, *J. Electrochem. Soc.*, **165**, A1529–A1536 (2018).

57. L. myguysolutions com My Guy Solutions, https://www.virtual-ii.com/product_info.php?products_id=107&osCsid=d104ba638466392a3c6a36b61db993f8.

58. D. Y. Wang, N. N. Sinha, R. Petibon, J. C. Burns, and J. R. Dahn, *Journal of Power Sources*, **251**, 311–318 (2014). (accessed on December 14, 2018)

59. D. Y. Wang, J. Xia, L. Ma, K. J. Nelson, J. E. Harlow, D. Xiong, L. E. Downie, R. Petibon, J. C. Burns, A. Xiao, W. M. Lamanna, and J. R. Dahn, *J. Electrochem. Soc.*, **161**, A1818–A1827 (2014).

60. C. P. Aiken, J. Self, R. Petibon, X. Xia, J. M. Paulsen, and J. R. Dahn, *J. Electrochem. Soc.*, **162**, A760–A767 (2015).

61. R. Petibon, V. L. Chevrier, C. P. Aiken, D. S. Hall, S. R. Hyatt, R. Shunmugasundaram, and J. R. Dahn, *J. Electrochem. Soc.*, **163**, A1146–A1156 (2016).

62. D. J. Xiong, R. Petibon, M. Nie, L. Ma, J. Xia, and J. R. Dahn, *Journal of The Electrochemical Society*, **163**, A546–A551 (2016).

63. E. Björklund, D. Brandell, M. Hahlin, K. Edström, and R. Younesi, *Journal of The Electrochemical Society*, **164**, A3054–A3059 (2017).

64. B. R. Long, S. G. Rinaldo, K. G. Gallagher, D. W. Dees, S. E. Trask, B. J. Polzin, A. N. Jansen, D. P. Abraham, I. Bloom, J. Bareño, and J. R. Croy, *Journal of The Electrochemical Society*, **163**, A2999–A3009 (2016).

65. Q. Liu, C. Du, B. Shen, P. Zuo, X. Cheng, Y. Ma, G. Yin, and Y. Gao, *RSC Advances*, **6**, 88683–88700 (2016).

66. F. Dogan, J. T. Vaughey, H. Iddir, and B. Key, *ACS Appl. Mater. Interfaces*, **8**, 16708–16717 (2016).

67. N. Leifer, O. Srur-Lavi, I. Matlahov, B. Markovsky, D. Aurbach, and G. Goobes, *Chemistry of Materials*, **28**, 7594–7604 (2016).

68. F. Zhou, X. Zhao, and J. R. Dahn, *J. Electrochem. Soc.*, **157**, A798–A801 (2010).

69. https://srdata.nist.gov/xps/.

70. T. A. Carlson and G. E. McGuire, *Journal of Electron Spectroscopy and Related Phenomena*, **1**, 161–168 (1972).

71. B. R. Strohmeier, *Surface and Interface Analysis*, **15**, 51–56 (1990).

72. D. Mohanty, K. Dahlberg, D. M. King, L. A. David, A. S. Sefat, D. L. Wood, C. Daniel, S. Dhar, V. Mahajan, M. Lee, and F. Albano, *Scientific Reports*, **6**, 26532 (2016).

73. J. W. Kim, J. J. Travis, E. Hu, K.-W. Nam, S. C. Kim, C. S. Kang, J.-H. Woo, X.-Q. Yang, S. M. George, K. H. Oh, S.-J. Cho, and S.-H. Lee, *Journal of Power Sources*, **254**, 190–197 (2014).

74. Q. Q. Liu, L. Ma, C. Y. Du, and J. R. Dahn, *Electrochimica Acta*, **263**, 237–248 (2018).

75. L. Ma, L. Ellis, S. L. Glazier, X. Ma, Q. Liu, J. Li, and J. R. Dahn, *J. Electrochem. Soc.*, **165**, A891–A899 (2018).

APPENDIX A SUPPLEMENTAL INFORMATION

Direct excitation of ^{27}Al nuclei is unsuitable for the analysis of many samples because the sample signal is frequently convoluted with strong background signals from the rotor and static probe head components. One approach is to use a Hahn-echo excitation pulse sequence in order to minimize the background signals. However, for the samples in this work, the Hahn-echo sequence had the unwanted result of also affecting the signal from the actual sample. Therefore, samples were measured via direct excitation and the background signal from the empty rotor and probe head components was manually subtracted. This involved careful adjustment of the intensity, such that the subtraction mostly corrects for the electronic ringing that causes the baseline rolling and gave as flat as possible baselines. Additional baseline rolls were removed by spline fitting. This procedure is illustrated for the as-received Al_2O_3-coated NMC material in Figure B.1. The resulting spectra for all samples are shown in Figure B.2. It can be seen that the background subtraction is imperfect near the center of the spectra, making this region unreliable. However, the spinning sidebands are nonetheless useful for performing analysis on the Al_2O_3 coatings.

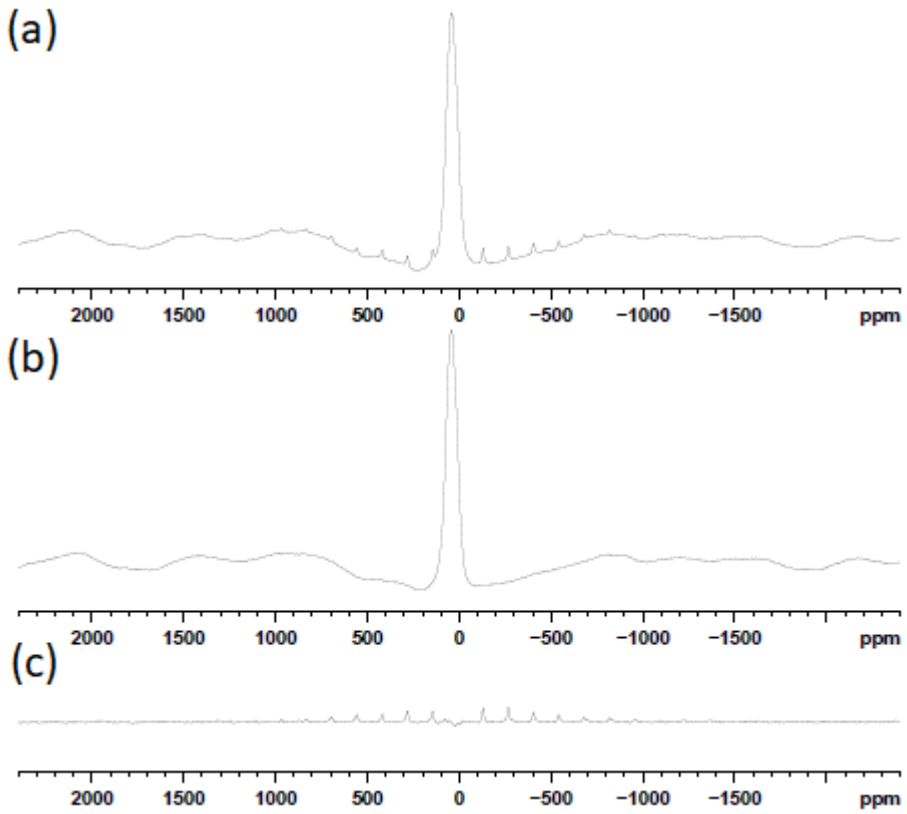

Figure A.1: 27Al MAS ssNMR spectra of a) as-received Al_2O_3-coated NMC622, b) background signal of the empty rotor and probe head components, and c) difference between spectrum (a) and spectrum (b) . The intensity of the background signal was adjusted to give as flat a baseline as possible.

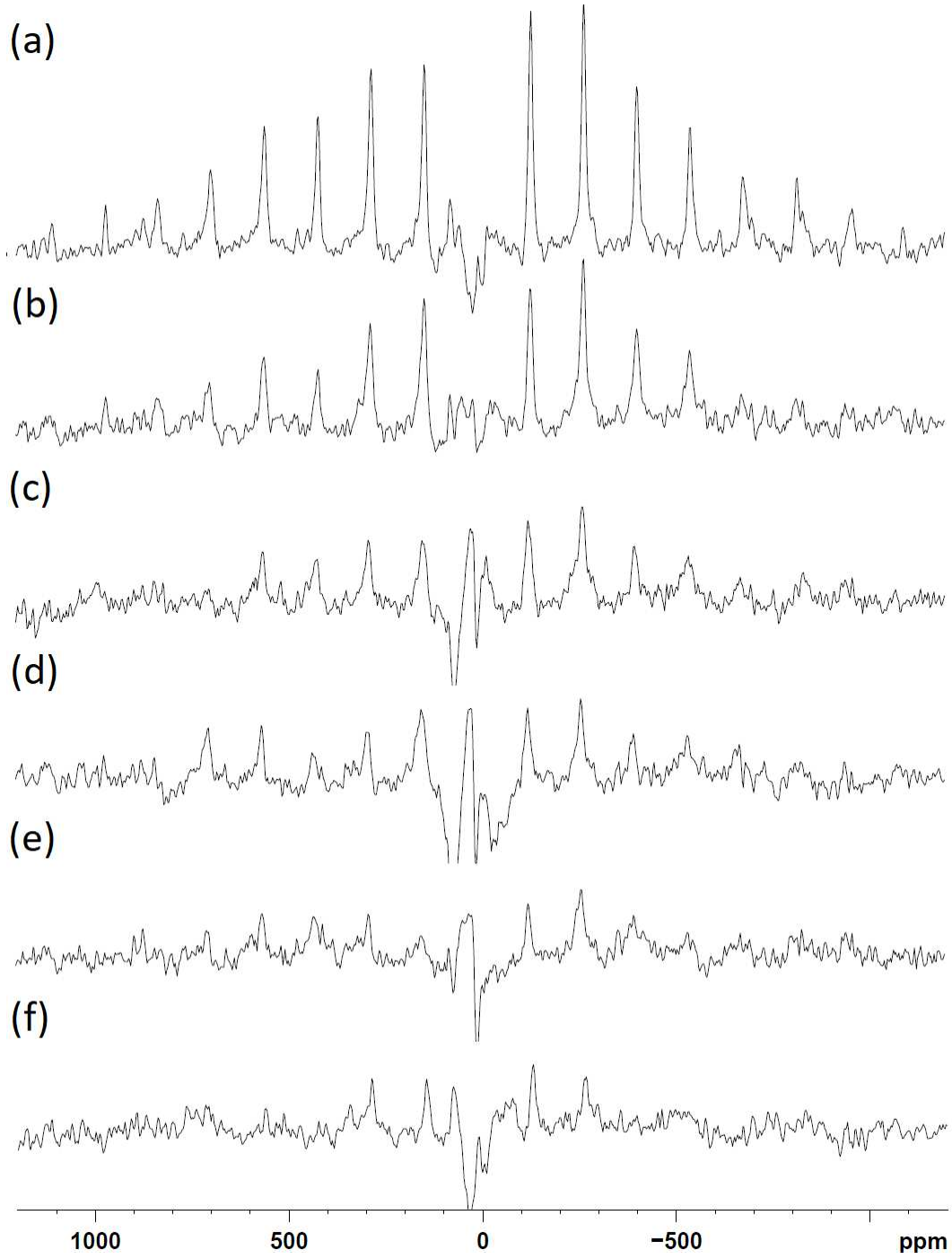

Figure A.2: Background-corrected 27Al ssNMR spectra of Al_2O_3-coated NMC622 material a) as-received and annealed at b) 400°C, c) 500°C, d) 600°C, e) 700°C, and f) 900°C.

APPENDIX B LICENSE AGREEMENT

ELSEVIER LICENSE
TERMS AND CONDITIONS

Mar 06, 2019

This Agreement between Ms. Vivian Murray ("You") and Elsevier ("Elsevier") consists of your license details and the terms and conditions provided by Elsevier and Copyright Clearance Center.

License Number	4543160064064
License date	Mar 06, 2019
Licensed Content Publisher	Elsevier
Licensed Content Publication	Materials Chemistry and Physics
Licensed Content Title	Preparation of Li–Al–O films by laser chemical vapor deposition
Licensed Content Author	Chen Chi,Hirokazu Katsui,Rong Tu,Takashi Goto
Licensed Content Date	Feb 14, 2014
Licensed Content Volume	143
Licensed Content Issue	3
Licensed Content Pages	6
Start Page	1338
End Page	1343
Type of Use	reuse in a thesis/dissertation
Portion	figures/tables/illustrations
Number of figures/tables/illustrations	1
Format	both print and electronic
Are you the author of this Elsevier article?	No
Will you be translating?	No
Original figure numbers	Figure 5
Title of your thesis/dissertation	Studying the Diffusion of Al3 ions from Atomic Layer Deposited Al2O3 Surface Coatings into Positive Electrode Materials and the Effects Thereof Using Full Coin Cells
Expected completion date	Mar 2019
Estimated size (number of pages)	50
Requestor Location	Ms. Vivian Murray 5264 Morris St.